Oncken, O., Boutelier, D., Dresen, G., Schemmann, K. (2012): Strain accumulation controls failure of a plate boundary zone: Linking deformation of the Central Andes and lithosphere mechanics. - Geochemistry Geophysics Geosystems (G3), 13, 12

DOI: 10.1029/2012GC004280

Geochemistry Geophysics Geosystems G3

Article
Volume 13, Number 12
22 December 2012
Q12007, doi:10.1029/2012GC004280
ISSN: 1525-2027

Published by AGU and the Geochemical Society

Strain accumulation controls failure of a plate boundary zone: Linking deformation of the Central Andes and lithosphere mechanics

O. Oncken
Helmholtz Centre Potsdam, GFZ German Research Centre for Geosciences, Telegrafenberg, DE-14473 Potsdam, Germany (oncken@gfz-potsdam.de)

D. Boutelier
School of Geosciences, Monash University, Clayton, Victoria 3800, Australia

G. Dresen
Helmholtz Centre Potsdam, GFZ German Research Centre for Geosciences, Telegrafenberg, DE-14473 Potsdam, Germany

K. Schemmann
Statoil ASA, NO-4035 Stavanger, Norway

[1] We make use of observations on orogenic strain accumulation and deformation partitioning in the Central Andes to explore the backarc strength evolution at the lithospheric scale. In plan view, the Altiplano-Puna plateaux experienced rapid initial increase of surface area undergoing active deformation during the Cenozoic. Beyond the maximum lateral extent reached around 10–15 Ma (40–50% of entire proto-Andes undergoing deformation) at 10–20% total strain, rapid localization initiated at the eastern flank of the Altiplano (Inter- and Subandean thrust belt) but not at the Puna latitude. Localization was associated with a significant increase in bulk shortening rate. Average fault slip rates equally increased by an order of magnitude following a protracted period of stable average rates. Estimates of strength evolution based on force balance calculations and critical wedge analysis suggest significant backarc weakening driving this change after the Middle Miocene. Strain accumulation led to localization and weakening with development of a detachment propagating through crust and upper mantle. We find that lithosphere-scale failure resulting from strain weakening beyond a critical strain threshold (c. 20%) and fault coalescence with formation of a weak detachment in shales (effective coefficient of friction < 0.1) plays a key role in the evolution of the Andes. Strain-related lithosphere weakening appears to dominate over the impact of external forcing mechanisms, such as variations of plate convergence, mantle-assisted processes, or erosion. Comparison of these orogen-scale observations with experimental rock rheology indicates substantial similarity of deformation behavior with similar weakening thresholds across a wide range of scales.

Components: 14,000 words, 8 figures, 3 tables.

Keywords: Andes; deformation analysis; localization; plateau formation; weakening.

Index Terms: 8031 Structural Geology: Rheology: crust and lithosphere (8159); 8102 Tectonophysics: Continental contractional orogenic belts and inversion tectonics; 8118 Tectonophysics: Dynamics and mechanics of faulting (8004).

Received 7 June 2012; **Revised** 31 October 2012; **Accepted** 2 November 2012; **Published** 22 December 2012.

Oncken, O., D. Boutelier, G. Dresen, and K. Schemmann (2012), Strain accumulation controls failure of a plate boundary zone: Linking deformation of the Central Andes and lithosphere mechanics, *Geochem. Geophys. Geosyst.*, *13*, Q12007, doi:10.1029/2012GC004280.

1. Introduction

[2] Strain localization is a fundamental process affecting Earth materials irrespective of the rheological regime. It has been reported from deformation experiments to be usually associated with a drop in material strength [e.g., *Paterson*, 1978; *Lockner et al.*, 1991; *Scholz*, 2002; *Stanchits et al.*, 2005; *Karato*, 2008]. In numerical studies and statistical analysis of deformation *Spyropoulos et al.* [2002] [see also *Lyakhovsky et al.*, 2001] have shown that slip weakening is associated with progressive crack coalescence and localization. In the ductile field, an increasing wealth of field observations from the scale of rock fabrics to individual faults, shear zones or even networks of the latter underpin the important role of varying weakening mechanisms [e.g., *White et al.*, 1980; *Hobbs et al.*, 1990; *Drury and Urai*, 1990; *Fusseis et al.*, 2006; *Handy et al.*, 2007; *Hansen et al.*, 2012; *Vauchez et al.*, 2012, and references therein]. From these studies, localization is often manifested by an initial stage of dilatancy and lateral spreading of the deforming zones – often involving hardening – succeeded by progressive localization of deformation and coalescence of shear bands and fractures to form throughgoing shears.

[3] The scale-dependence of processes leading to strain localization is largely unknown. In particular, little is known on the evolution of entire fault networks or plate boundary zones in contrast to individual shear zones due to a lack of data. *McLeod et al.* [2000] and *Cowie et al.* [2005] summarize observations on the evolution of extensional structures forming the North Sea Basin. The latter clearly exhibits a trend toward progressive fault coalescence and localization of deformation over several 10 Myrs associated with accelerated fault slip. However, the cause for slip acceleration remains ambiguous. In a review, *Ben-Zion and Sammis* [2003] argue that any fault system involving weakening is prone to develop toward a more simple and localized pattern of strain accumulation.

[4] The very large scale under consideration involving the entire lithosphere introduces at least two fundamental obstacles:1) Collection of high resolution data (spatial resolution and temporal evolution) at sufficiently long time scales is usually restricted to small parts of the lithosphere, 2) the mechanical response of a stratified lithosphere with largely unknown composition and evolving thermal structure is likely governed by superposition of transient processes operating on various time scales that are difficult to resolve at present but more so in the geological past. Moreover, while experimental and fabric studies provide clear evidence for the operation of a few key processes in controlling localization (e.g., fracture and dilatancy enabling enhanced fluid-rock interaction, grain size reduction, etc.), how it occurs at the large scale may be quite different [e.g., *Handy et al.*, 2007; *Gerbi et al.*, 2010]. Large scale mechanical heterogeneities and structural inheritance, local to regional perturbations of the thermal state due to active geodynamic processes, changes in plate convergence parameters or body forces affecting the force balance and its local variations, and more, may all affect localization and strength evolution. Although a number of studies exist investigating the development of shear zones and shear zone networks based on field work and numerical modeling, ranging in scale from outcrop to lithospheric [e.g., *Vissers et al.*, 1995; *Ben-Zion and Sammis*, 2003; *Fusseis et al.*, 2006, and references therein], we are not aware of field studies highlighting strain localization at the lithospheric scale that also provides bounds on the varying strength of an evolving large-scale shear zone system.

[5] We use records from the central Andes to monitor changing deformation patterns during plate convergence and formation of a high plateau. These records represent one of the best resolved data on long-term orogenic deformation accumulation. Here we focus on deformation patterns and strength evolution to explore the upper plate response during plate convergence and subduction rather than focusing on the various mechanisms of external forcing of upper plate deformation and plateau uplift usually studied [e.g., *Oncken et al.*, 2006; *Barnes and Ehlers*, 2009; *Capitanio et al.*, 2011, and references therein].

2. Geological Framework

2.1. Structure and Evolution of the Central Andes

[6] The evolution of the modern Central Andean Cordillera started in Early Tertiary times with focused plateau development since the Middle to

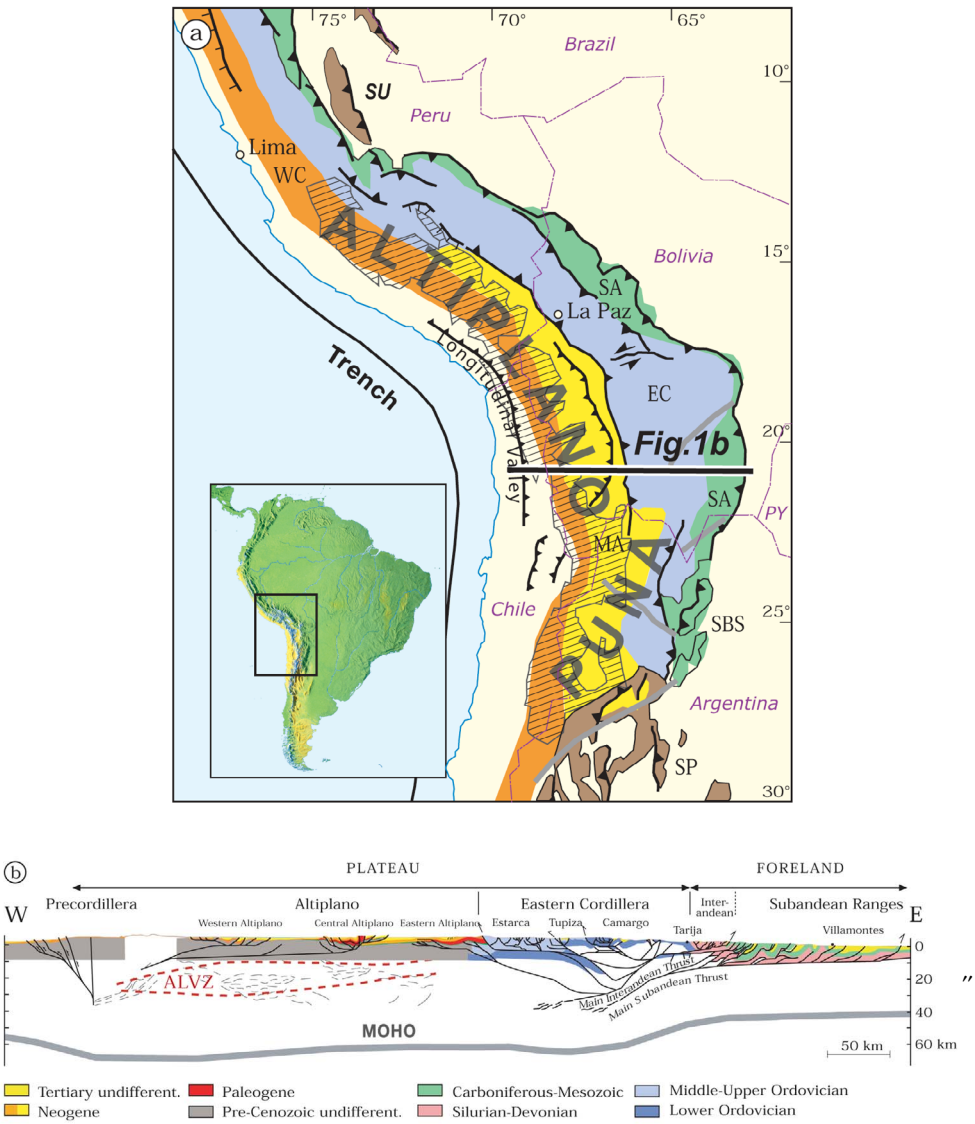

Figure 1. (a) Tectonic map of central Andes (modified from *Oncken et al.* [2006]). Map shows outline of major tectonic units SBS – Santa Barbara System, SP – Sierras Pampeanas, SU – Shira uplift, SA – Sub-Andean Belt, EC – Eastern Cordillera, MA – magmatic arc (striped zone), WC – Western Cordillera, LV – Longitudinal Valley. (b) Cross section at 21°S (modified from *Oncken et al.* [2006]) integrating geological surface observations and geophysical data for mid-crustal features (ALVZ – Altiplano low velocity zone) and Moho. The Interandean belt shown in the section occupies the eastern rim of the eastern Cordillera in Figure 1a.

Late Miocene [e.g., *Allmendinger and Gubbels*, 1996; *Allmendinger et al.*, 1997; *Lamb and Hoke*, 1997; *Elger et al.*, 2005; *Oncken et al.*, 2006; *Barnes and Ehlers*, 2009; *Carrapa et al.*, 2011]. This period of plateau growth shows a complex lateral and temporal pattern of deformation accumulation [*Oncken et al.*, 2006, and references therein]. After an earlier stage of shortening that started in Paleogene times in the west, deformation involved the proto-Eastern Cordillera and proto-plateau region since ≥40 Ma. Since ~15 Ma, the zone of active shortening migrated from the plateau into the Subandean thrust belt. Deformation in the plateau domain largely stopped by 7 Ma. During this evolution, the convergence rate between the Nazca and South America plates underwent continuous slowing from a peak of ~15 cm/a during the early Miocene [*DeMets et al.*, 1990; *Sdrolias and Müller*, 2006] to the present value of 6.6 cm/a from GPS data [*Angermann et al.*, 1999].

[7] This evolution of deformation resulted in the formation of major structural units trending approximately parallel to the mountain range (Figure 1a).

Except for the Altiplano-Puna plateau that begins near 14°S in southern Peru and terminates near 27°S in northern Argentina, these units can be traced along the entire central segment of the Andean chain. The only mildly deformed "western monocline" or Altiplano west flank, links the Longitudinal Valley at c. One km elevation with the plateau at ~4 km altitude [*Isacks*, 1988; *Victor et al.*, 2004]. The Western Cordillera superseding the rim of this flank comprises the volcanic arc. Only minor Eocene to Late Miocene shortening has been observed from exposed areas east (some thrusting and folding) and west (formation of positive flower structure associated to Precordilleran Fault System) of the present arc [*Scheuber and Reutter*, 1992; *Haschke and Günther*, 2003; *Elger et al.*, 2005; *Charrier et al.*, 2005]. This observation provides a bound for any additional shortening hidden below the arc itself.

[8] The backarc formed by the Altiplano-Puna plateaux and the Eastern Cordillera shows Cenozoic west- and east-vergent thrusting and folding. At the eastern plateau flank, the Interandean and Subandean belt form a thin-skinned east-facing foreland fold-and-thrust belt from Peru to northernmost Argentina (Figure 1b). The positions of the major detachment horizons are controlled stratigraphically and are mostly located in Palaeozoic shales near the base of a thick sedimentary cover. From northern Argentina southward, the structural style of foreland thrusting changes to thick-skinned inversion structures and further south to large-scale basement thrusts. These form a broken foreland as in the Sierras Pampeanas and along the margin of the Puna. Similar foreland basement thrusts but of smaller size also occur in Peru, e.g., the Shira uplift [*Cristallini et al.*, 1997; *Kley and Monaldi*, 2002; *Carrapa et al.*, 2011; *Devlin et al.*, 2012].

[9] Crustal shortening and plateau evolution is confined to the backarc area (Figure 1b) where the thin skinned fold and thrust belt of the Eastern Cordillera and Subandean belt accumulated ~150–200 km of shortening [*Kley and Monaldi*, 1998; *Baby et al.*, 1997] compared to ~85 km shortening in the plateau itself [*Lamb and Hoke*, 1997; *Lamb*, 2000; *Elger et al.*, 2005]. In contrast to the more symmetrically deformed Puna plateau, the Altiplano has been suggested to be the result of simple shear crustal thickening from westward underthrusting of the Altiplano area by the Brazilian shield [e.g., *Allmendinger and Gubbels*, 1996; *Allmendinger et al.*, 1997]. Associated isostatic surface uplift has created the present-day plateau with an average elevation of 3800 m for the Altiplano and 4500 m for the Puna plateau. Based on a variety of techniques, uplift evolution has been reconstructed along two contrasting model paths, exhibiting either gradual uplift over time, or a rapid rise after 10 Ma [e.g., *Gregory-Wodzicki*, 2000; *Sobolev and Babeyko*, 2005; *Garzione et al.*, 2006, 2008; *Hoke and Garzione*, 2008; *Barnes and Ehlers*, 2009, and references therein]. These various uplift models and their relation to the evolution of shortening remain a matter of debate.

2.2. Active Tectonics and Seismicity

[10] GPS shortening rates (data from *Bevis et al.* [2001] and *Klotz et al.* [2006]) compare with the geological estimates revealing current shortening rates across the Subandean belt from 6.5 to 13 mm/yr focused near its front [*Bevis et al.*, 2001; *Brooks et al.*, 2011]. Slip is localized on a basal detachment forming the root of a set of frontal thrusts [e.g., *Baby et al.*, 1992, 1997; *Kley*, 1996; *Allmendinger and Gubbels*, 1996], which are believed to be currently locked [*Brooks et al.*, 2011]. Seismic activity clusters along the frontal thrust system (Figure 2) and focal mechanisms suggest thrusting toward the foreland (maximum depth of seismicity shown <50 km). These focal mechanisms and stress data from the World Stress Map indicate that the maximum horizontal stress directions are generally oriented subnormal to the arcuate Subandean belt [*Heidbach et al.*, 2010]. In contrast, GPS vectors mostly show an ENE-WSW orientation parallel to the convergence vector between the Nazca and South American plates (Figure 2). This implies that the kinematics between the main Andean orogenic body constituting the upper plate from the forearc to the Subandean thrust belt and the South American lower plate foreland differ significantly. *Brooks et al.* [2003] have, therefore, suggested treating the main Andean body as an independent microplate.

3. Kinematic Analysis

3.1. Methods

3.1.1. Spatial Deformation Pattern Based on Geological Observations

[11] We present the evolving deformation pattern of the Central Andes by monitoring the change in area fraction that was actively deformed during a given time period. The reference frame is the area of the Central Andes and the width of the mountain chain between the Longitudinal Valley in the west and the eastern foreland. For the analysis of the spatial

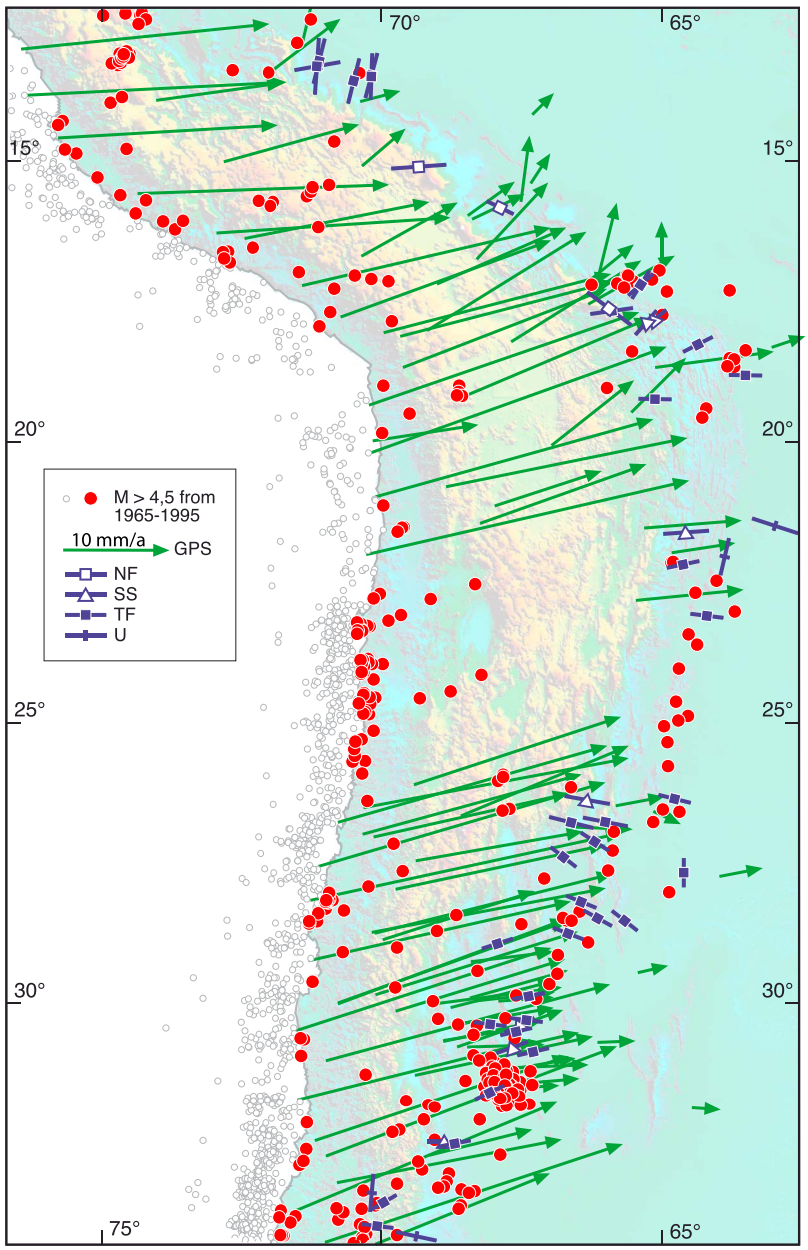

Figure 2. Central Andes map showing GPS displacement (from *Allmendinger et al.* [2005], based on *Kendrick et al.* [2001] and *Brooks et al.* [2003]), crustal seismicity, 1965–1995, from depths <50 km (from database of *Engdahl et al.* [1998]; plate interface earthquakes shown in small symbols) and $S_H$max stress axes (maximum horizontal stress) on eastern flank of Andes and foreland from World Stress Map project [*Heidbach et al.*, 2010] (NF: normal faulting; SS: strike slip faulting; TF: thrust faulting; U: undetermined regime). Note change in orientation of GPS vectors and stress axes at and east of eastern deformation front.

distribution of deformation accumulation we use the database compiled by *Oncken et al.* [2006] (complemented by more recent published data; see Tables 1 and 2) that covers the Central Andean evolution throughout the Cenozoic. Each data set defines the geographic coordinates of the area or geologic structure studied, the start and end of deformation activity in Myrs as found from dating various deformation-related features. We take into account only those references that precisely document the location of the study area, the position and processing of samples, and the dating method applied. Data covers almost the entire area, except for some regions within the western parts of the

Table 1. Compilation of Shortening Data (in km) Sorted by Structural Units and Latitudinal Domains

° S Lat.	Pacific Piedmont	Altiplano-Puna; West. Cordillera	Eastern Cordillera	Foreland Belt[a]	Total[b]	Total, Preferred	Shortening Cross-Sectional Area[c]	References
15	15[d]	15–40	123	100–121	248–294	270	270[c]	*Baby et al.* [1989, 1997]; *Roeder and Chamberlain* [1995]; *Rodriguez et al.* [2001]; *McQuarrie et al.* [2008]
18	14–16	14–47	>132	90[e]–135	>241–330	265–320	275[c]	*Sheffels* [1990]; *Baby et al.* [1993, 1997]; *Roeder and Chamberlain* [1995]; *Muñoz and Charrier* [1996]; *McQuarrie and DeCelles* [2001]; *García et al.* [2002]; *Haschke and Günther* [2003]
20–21	13–18	60	35–95	96–135	204–308	280	320[c]	*Hérail et al.* [1990]; *Baby et al.* [1992]; *Dunn et al.* [1995]; *Kley* [1996]; *McQuarrie and DeCelles* [2001]; *Müller et al.* [2002]; *Victor et al.* [2004]; *Elger et al.* [2005]; *Uba et al.* [2009]; *Haschke and Günther* [2003]
24–26	14–18[d]	30–50	40–60[d]	21–30	95–148	135 100–160[c]	260[c]	*Grier et al.* [1991]; *Cladouhos et al.* [1994]; *Cristallini et al.* [1997]; *Coutand et al.* [1999]; *Kley and Monaldi* [2002]

[a]Including Interandean zone.
[b]Range results from summing values given for individual units in left columns.
[c]Data from *Kley and Monaldi* [1998] and *Vietor and Echtler* [2006].
[d]Estimated from average shortening ratio of unit along strike when associated to similar elevation.
[e]Measured from cross-section (no value given in ref.) or alternative estimate (this paper).

Table 2. Compilation of Shortening Age Periods (in Ma) Sorted by Structural Units and Latitudinal Domains

° S Lat.	Pacific Piedmont	West Cordillera	Altiplano-Puna	Eastern Cordillera	Foreland Belt	References
15	44–38 25–8 3–1	40–6	27–8 5–1	45–25 (25–15) 15–1	15–0	*Mercier et al.* [1992]; *Baby et al.* [1997]; *Cristallini et al.* [1997]; *Kley and Monaldi* [2002]; *Rousse et al.* [2005]; *Ruiz et al.* [2009]; *Barnes et al.* [2006]; *McQuarrie et al.* [2008]; *Schildgen et al.* [2009]
18	44–38 28–6	22–7	28–5 5–0	45–17	15–0	*Hérail et al.* [1996]; *Muñoz and Charrier* [1996]; *Baby et al.* [1997]; *Lamb and Hoke* [1997]; *García et al.* [2002]; *Kley and Monaldi* [2002]; *Elger et al.* [2005]; *Rousse et al.* [2005]; *Charrier et al.* [2005]; *Barnes et al.* [2008]
20–21	44–38 28–6	22–7	28–5	45–17	15–0	detailed compilation and ref. in *Elger et al.* [2005] and *Oncken et al.* [2006]; *Haschke and Günther* [2003]; *Barnes et al.* [2008]; *Uba et al.* [2009]
24–26	46–38 18–0	46–38 18–0	29–0	40–33 20–1	28–11 4–0	*Marrett et al.* [1994]; *Cristallini et al.* [1997]; *Coutand et al.* [1999, 2001]; *Kley and Monaldi* [2002]; *Jordan et al.* [2010]; *Carrapa et al.* [2005, 2011]

Altiplano/Western Cordillera and northern Puna (between 18.5 and 19.5°S and 22.5–23.5°S) (see Figure 3).

[12] The above database is highly heterogeneous in terms of size of study areas, their spatial distribution, and resolution of structures analyzed. We therefore gridded the entire study area to achieve a more homogeneous coverage (see Figure 3). We defined a point spacing of 40 km in this grid because that is: a) the smallest study areas in our database; b) and the lower limit of the characteristic length of map-scale tectonic structures forming the units reflecting deformation (fault lengths, wavelength of map-scale folds). Based on the above database, we assign each grid point the published information on deformation activity (within a radius of 20 km) using time bins of 1 Myrs starting in the Eocene. This ultimately results in a data set of ~440 nominal values for the plateau area indicating active or no deformation for each Myrs of the past 50 Myrs. For more detailed inspection, we also break down this total number into individual transects (at 15–16, 18, 21, and 25°S) of approximately 2° width for each transect (Figure 3).

[13] While age data occasionally provide a temporal resolution of some 10^5 yrs., estimating the start and end of deformation for each location has a higher uncertainty (see *Elger et al.* [2005] for discussion). Hence, while we sampled the above data in 1 Myr time bins, we allow for larger uncertainty in identifying these ages by adding the isotopic age errors to the deformation periods. This effectively limits resolution to 2–3 Myrs, but also reduces artifacts from limitations of age dating.

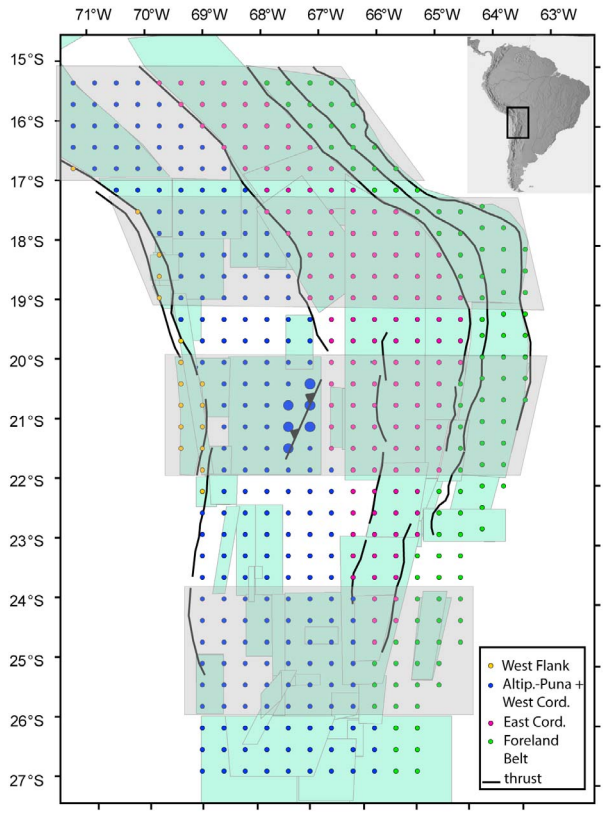

Figure 3. Grid map used for binning of data. Points are assigned the local age information on deformation timing (see text). Green shaded areas show areas covered by data on deformation ages in data bank. Transects and swaths shown in gray shade indicate data collected for the individual transects in Figure 4a. Example structure shows Uyuni-Khenayani fault zone and the 6 major grid points that would reflect its activity as identified in the study by *Elger et al.* [2005] (see text for detailed description).

[14] As an example, we show treatment of the data for the Uyuni-Khenayani Fault structure in the Southern Altiplano [*Elger et al.*, 2005]: The structure – and the grid points carrying the information – is shown in Figure 3 including the deformed hangingwall. From dating of syntectonic deposits, undeformed volcanoes crossing the faults, analysis of reflection seismic data and section balancing, the authors identified faulting to have been active at some time between 33 and 27 Ma (defined by initiation of cooling and first dated posttectonic deposit), followed by a lull of no to very slow slip. Reactivation occurred shortly before c. 14 Ma and activity terminated at 10 Ma (as seen from initiation of renewed syntectonic sedimentation and posttectonic sedimentary overlap). The uncertainty in defining the onset of deformation is due to uncertainty in fission track dating [*Ege et al.*, 2007] of basement exhumation and few datable ash deposits in the Oligocene deposits (in this case we estimate the uncertainty to be ± 2 Myrs). Uncertainty in defining the end of activity is lower than 1 Myrs (error of isotopic dating of undeformed volcanics unconformably overlying Late Miocene syntectonic deposits). The 6 points covering this particular fault and hangingwall unit (see Figure 3) define a patch indicating locally active deformation in the above time windows and inactivity for the remaining times.

[15] For the plateau and the above 4 transects, the points active per Ma define the fraction of the total area of the plateau and the individual transect, undergoing deformation during one time increment. The resulting spatial and temporal evolution of deformation distribution is shown as an animated sequence in the auxiliary material (Animation S1) that also contains a detailed discussion of uncertainties.[1]

3.1.2. Assessing Shortening Rate

[16] We also estimated shortening velocities for various time periods at several latitudes. From more detailed studies [*Victor et al.*, 2004; *Elger et al.*, 2005], temporal resolution of accumulation of deformation at 21°S with up to 1 Myrs for individual faults is significantly higher than at other latitudes. The shortening rates shown for 21°S from *Oncken et al.* [2006] have been improved by including recent age dating for the Eastern Cordillera and Interandean belt by *Barnes et al.* [2008] and for the Subandean belt by *Uba et al.* [2009]. We sampled three other sections at 15, 18 and 25°S (see Figure 3 for location of sampled corridors) using published data (Figures 4a and 4c; see also *Oncken et al.* [2006]; see summary in Table 1). For the three additional transects, we use the data shown in Tables 1 and 2. We linearly averaged shortening for each domain (Table 1) over the active deformation period identified by the authors (Table 2). Details of the procedure and the uncertainties involved in estimating shortening magnitudes and rates are described in the auxiliary material.

3.2. Results

3.2.1. Spatiotemporal Deformation Pattern of the Central Andes Since 50 Ma

[17] Shortening rates across the Andes change abruptly through time in all transects (Figure 4). Within error introduced by deformation dating (see above) these stages are fairly well synchronized along strike for the Altiplano (14–22°S; Figure 4a). Shortening begins between 45 and 50 Ma with gradually or stepwise increasing rates. A significant increase in shortening rates to 4–9 mm/a across the entire Andes is found at some 32–27 Ma. Subsequently, rates fluctuate and decrease slightly until some 15 Ma ago but then suddenly increase to the present-day shortening rates of 8–14 mm/a. This is interrupted, possibly, by a slower phase in the Pliocene. For the Puna Plateau rates are lower with only minor recent acceleration.

[18] The spatiotemporal deformation pattern, is represented by the orogen area fraction deforming during a 1 Myr time interval. The changing deformation pattern is related to the shortening rate evolution. To highlight these variations, we sampled these data separately for the Altiplano and the Puna plateau from the gridded maps (see Figure 3) and calculate them with respect to the present-day extent of the orogen. Increasing shortening rate at some 45 and around 30 Ma is associated with a rapid increase in surface area fraction undergoing deformation (Figures 4b and 4c). In contrast, immediately prior to the plateau-wide acceleration of shortening rate at 15–10 Ma, the actively deforming fraction of the plateau started decreasing. This change in trend is particularly pronounced in the Altiplano area but is less clear in the Puna transect. The drop in actively deforming area (Figure 4b) represents a conservative estimate of the deforming area fraction . At lower spatial coverage of age data deformation activity is assigned to entire structural units effectively increasing the size of an active area. For example, in the Subandean Belt recent deformation

[1] Auxiliary materials are available in the HTML. doi:10.1029/2012GC004280.

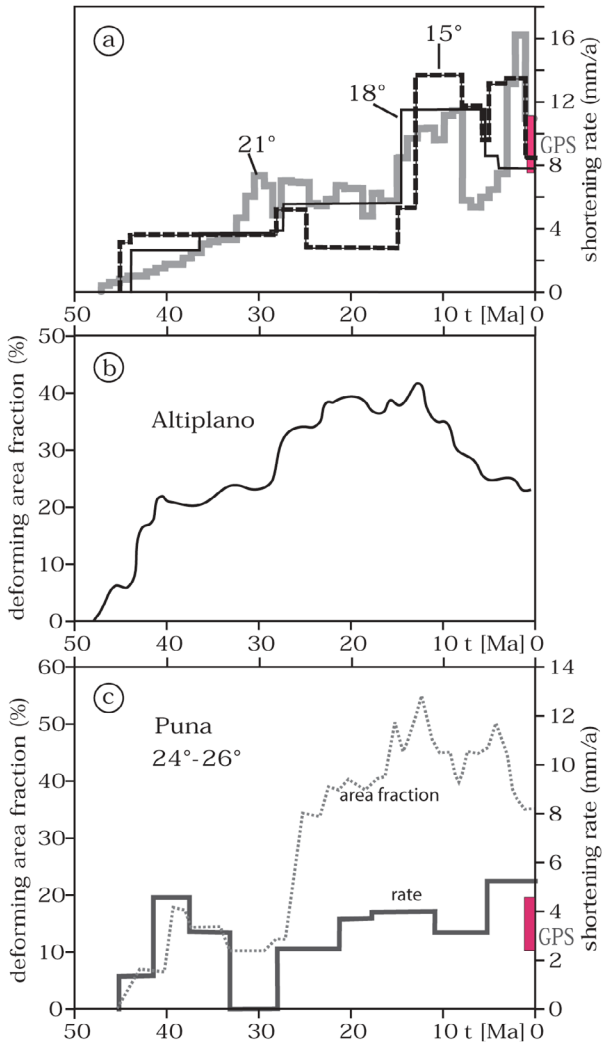

Figure 4. Shortening evolution in the Central Andes. (a) Central Andes shortening velocities from sections at 15, 18, 21°S for the Cenozoic covering the entire plateau and its flanks. Section at 21° updated from *Oncken et al.* [2006] integrating new data by *Barnes et al.* [2008] and *Uba et al.* [2009]. Sections at 15 and 18°S calculated from data shown in Tables 1 and 2 (see text for details). (b) Evolution of percentage of Altiplano total surface area (14–22°S; ratio of grid points with active deformation versus total number of grid points) undergoing shortening during the Cenozoic in 1 Myr time steps. (c) Shortening rate for the entire orogen at Puna latitude and percentage of total surface area (22–26°S) undergoing shortening during the Cenozoic; GPS velocities and associated uncertainty from *Bevis et al.* [2001] and *Klotz et al.* [2006].

is localized in a few frontal thrusts, but past faulting activity is still difficult to resolve in space and time. To summarize, during the earlier stages of shortening (Eocene to Mid-Miocene), deformation involved a progressively increasing area, whereas since the Middle Miocene deformation became increasingly localized toward the eastern foreland.

[19] The change in area fraction undergoing deformation evolves with the horizontal strain accumulated across the orogen (measured as magnitude of horizontal strain from balanced cross sections; see published database by *Oncken et al.* [2006], summarized in Table 1; uncertainties are discussed in auxiliary material). This is seen in all transects analyzed here (at 15–16, 18, 21, and 25°S; Figure 3). The deforming area first increased with accumulating strain in two stages to some 40–50% of the total surface area (Figure 5a). Increase in area undergoing deformation occurred by emergence of new active patches, their lateral growth and by their coalescence. Subsequently, deformation increasingly shifted toward the foreland reducing the actively deforming area for the Altiplano latitude to 20–30% and then remaining at this level. In the Puna transect (24–26°S), a decrease of actively deforming area has only started and not progressed to the stage of the Altiplano.

[20] For all transects, rapid initial increase of deformation area occurred at low strains of 1–3% only (Figure 5a; all strain values are calculated with respect to the restored initial width between the deformation fronts). A second increase in deforming area following minor localization only started at strains >5%. While we cannot exclude that this early feature may be an artifact from incomplete data on early deformation, we note that this trend appears in all transects suggesting it is a robust observation. Subsequently, deforming area gradually increased until a maximum was reached at 10–20% horizontal strain some 10–15 Ma ago. Subsequently, a change from increasing to decreasing area fraction of active deformation occurred.

[21] Addition of potentially undetected horizontal strain to the presented pattern will slightly shift the area fraction to higher values and will shift the maximum of spatial spreading of deformation (at 10–20% strain) to slightly higher strain values. However, we expect this effect to be minor as estimated upper crustal shortening magnitudes imply crustal thicknesses that are in good agreement with geophysically observed values [*Hindle et al.*, 2005].

3.2.2. Fault Number and Fault Slip Rate at 21°S

[22] The section at 21°S allows analyzing the deformation evolution locally at higher resolution (Figures 5b and 5c). We counted the number of major faults mapped (with >300 m displacement) and analyzed the data [see *Elger et al.*, 2005;

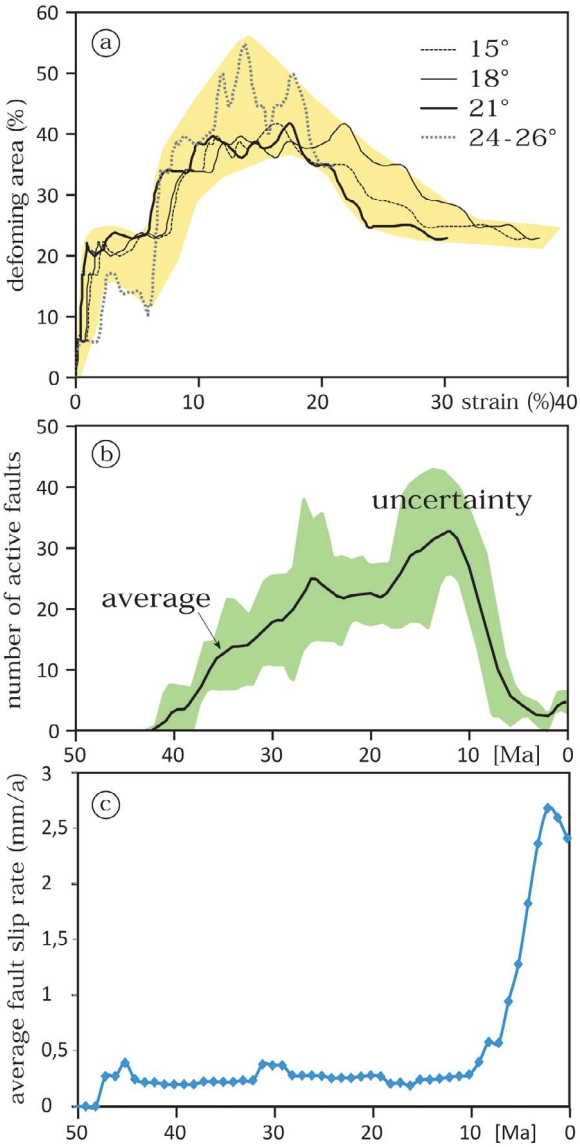

Figure 5. Evolution of deformation localization in the Central Andes. (a) Percentage of deforming area versus horizontal strain along several transects across the Altiplano and Puna domains. For each transect the ratio of actively deforming area (represented by point number) versus total area is collected in +/−1° corridors (see Figure 3 for locations). (b) Total number of active faults (with displacement >300 m) for transect at 21°S throughout the Cenozoic; uncertainty is mainly due to assessment of start and end of motion on individual faults [see *Elger et al.*, 2005; *Oncken et al.*, 2006]. Average is calculated from smoothing with 3 Myr sliding window. (c) Average fault slip rate at 21°S for the past 50 Myrs. We calculate this value for the incremental width of the growing orogen, the incremental deforming area and for averaged shortening across the Altiplano (15–22°S) assuming that the strain is focused entirely in active fault zones (using the fault number observed at 21°S).

Oncken et al., 2006] in time bins of one Myrs (Figure 5b). Where more detailed information on activity periods of individual faults is missing (Eastern Cordillera) we assume a similar ratio of active versus inactive faults for each fault system. The evolution of fault number and horizontal strain at 21°S both show a monotonic increase suggesting that shortening across the Central Andes is controlled by fault and shear zone evolution (Figure 5b). However, fault activity, i.e., active faults per time increment, clearly shows a significant drop starting at about 15–10 Ma. At this time, the number of faults actively accumulating slip decreased within a time frame of less than 10 Myrs from a total of ~38 faults (±10) to less than six major active faults (mostly in the Subandes). These faults not only accumulated the entire subsequent deformation, but also accommodate the elevated shortening rates until today. Finally, dividing the shortening rate by the number of active faults in 1 Myrs time steps, we find that the average horizontal contraction rate component of the faults increased from about 0.25 mm/a between 30 and 10 Ma by an order of magnitude to 2 to 3 mm/a in the Pliocene to present (Figure 5c).

4. Strength Analysis

[23] The observed localization of Miocene-to-recent deformation is associated with an increase in shortening rates. This implies a change in the external driving forces, or a reduction of backarc lithospheric strength, or both. Moreover, as first suggested by *Dalmayrac and Molnar* [1981], a change in the deformation pattern focusing shortening in a foreland thrust belt may also be due to an increase in buoyancy forces as the mountain chain rises and high plateaus form. To explore how these changes affect the observed kinematic pattern of the upper plate, we first analyze the role of uplift-controlled buoyancy changes for localization of deformation and then reconstruct the foreland wedge evolution to constrain potential changes in backarc strength.

4.1. Estimating Current Buoyancy and Horizontal Tectonic Forces

[24] The gradient in buoyancy forces across the mountain chain is usually employed to estimate the stresses operating on the plate boundaries [e.g., *Dalmayrac and Molnar*, 1981; *Molnar and Lyon-Caen*, 1988; *Lamb*, 2006; *Iaffaldano and Bunge*, 2008; *Meade and Conrad*, 2008]. The horizontal tectonic force resulting from plate convergence must at least balance the present-day buoyancy force in order to maintain the mountain range, which would

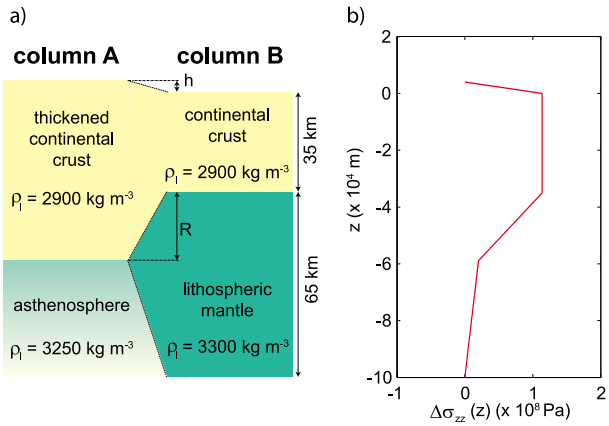

Figure 6. Model setup for estimate of buoyancy forces (see text for details). (a) Schematic lithospheric model setup used showing densities, initial thickness (on right side) elevation h, and crustal root R for foreland and plateau. (b) Difference in vertical traction σ_{zz} at depth z between the foreland and the high plateau as shown in Figure 6a.

otherwise collapse. Estimates of the average shear stresses at the plate boundary between the Nazca and South American plates are of the order of 35–40 MPa [*Lamb*, 2006; *Boutelier and Oncken*, 2010].

[25] We assume that the tectonic driving forces at the plate margin balance the sum of the buoyancy forces exerted by the plateau on the Subandean foreland that displays a current shortening of up to 10 mm/a. The weight per unit area of a column of rock with elevation h is supported by the vertical traction σ_{zz} on its base

$$\sigma_{zz}(z) = \int_{-h}^{z} -g\rho(z')dz'$$

where z is depth, z′ is the integration variable, and g is the gravitational acceleration. The buoyancy force F_b between two lithospheric columns corresponding to the "orogen" and the "foreland" (Figure 6a), with two different density structures, is obtained by integration of the difference in vertical traction over the lithospheric thickness [*Froidevaux and Isacks*, 1984]

$$F_b = \int_{-h}^{L} \Delta\sigma_{zz}(z)dz$$

where $\Delta\sigma_{zz}$(z) is the difference in vertical traction at depth z, and L is the thickness of the lithosphere.

[26] For the central Andes, seismological studies have shown that the high topography is underlain by thickened continental crust directly on top of the asthenospheric mantle, with almost no mantle lithosphere in between [*Tassara et al.*, 2006]. For the continental foreland bordering the back arc, we use a reference lithospheric column that is 100 km thick and contains a 35 km thick continental crust (Figure 6) in agreement with the results summarized in *Tassara et al.* [2006]. We further assume an averaged crustal density of 2900 kg m^{-3}, an averaged lithospheric mantle density of 3300 kg m^{-3}, and an averaged asthenosphere density of 3250 kg m^{-3} [*Tassara et al.*, 2006]. At elevation h of ~4000 m, assuming isostatic equilibrium, and a crust resting directly on the asthenosphere, these densities yield a crustal root of 24 km and a total crustal thickness of 63 km. This is in general agreement with seismological studies [*Yuan et al.*, 2000]. Using this density structure, we compute the difference in vertical traction at depth z between the foreland and the high plateau and integrate to obtain the buoyancy force per unit length of the orogen (Figure 6b).

[27] For the buoyancy force F_b we obtain a value of 6.2×10^{12} N m^{-1}. For comparison, *Molnar and Lyon-Caen* [1988] estimate 5.2×10^{12} N m^{-1} using a similar approach, while *Husson and Ricard* [2004] obtained $F_b = 1 \times 10^{13}$ N m^{-1}. A geoid anomaly N can be computed from the buoyancy force [*Froidevaux and Isacks*, 1984]:

$$N = F_b 2\pi G/g^2$$

where G is the gravitational constant. Our estimation of the buoyancy force yields a geoid anomaly of 27 m, which is in agreement with observation of a geoid anomaly of 25 m in the plateau area [*Chase et al.*, 2009].

4.2. Evolution of Buoyancy Force Through Geologic Time

[28] With the rise of the Andes, the buoyancy force in the plateau area has increased. This increase must have been balanced at each time step by the tectonic forces deriving from normal and shear stresses operating on the plate boundary. The evolution of paleoelevation serves as a proxy to estimate the changing body forces operating on the plateau margins. Since reconstructions of past elevations are subject to significant uncertainty, for simplicity, we here model the contribution of body forces using the end-member scenarios summarized by *Barnes and Ehlers* [2009]: 1. A low-elevation proto-plateau started rising rapidly at about 10 Ma reaching approximately present elevation at ca. 6 Ma. 2. Plateau uplift occurred rather gradually through time during the entire evolution of the Andes. In addition, we use a

Table 3. Description of Models Used for Possible Evolution of Elevation, Crustal Thickness and Buoyancy Force in Figure 7

Model Name	Model Input	Model Output
A1	No lithospheric mantle + steady topographic rise	Crustal thickness + buoyancy force
A2	No lithospheric mantle + rapid topographic rise	Crustal thickness + buoyancy force
B1	Homogeneous thickening + steady topographic rise	Crustal thickness + buoyancy force
B2	Homogeneous thickening + rapid topographic rise	Crustal thickness + buoyancy force
C1	Crustal thickening from shortening estimates + no lithospheric mantle	Topography + buoyancy force
C2	Crustal thickening from shortening estimates + homogeneous thickening	Topography + buoyancy force

crustal thickness evolution model derived from our shortening estimates. Calculating the associated range in buoyancy forces back in time, we present six possible evolutions of the buoyancy force (Table 3).

[29] Assuming isostasy we first compute the crustal thickness that matches each of the two end-member elevation models. In models A1 and A2, the lithospheric structure corresponds to a continental crust of variable thickness resting directly on the asthenosphere. Model A1 uses the "steady rise" elevation model from *Ehlers and Poulsen* [2009], derived from paleoclimate corrected paleoaltimetry while model A2 uses the "rapid rise" elevation model derived from paleobotany, $\delta^{18}O$ and clumped ^{13}C-^{18}C isotopes [*Gregory-Wodzicki*, 2000; *Garzione et al.*, 2006, *Ghosh et al.*, 2006] (see Figure 7a for both models). In models B1 and B2, we assume that at 50 Ma the crustal thickness was 35 km and elevation resulted from thinning of the lithospheric mantle. From a sensitivity study (see auxiliary material) we find that the initial value for the thickness of the crust at 50 Ma only has a minor influence on the buoyancy force evolutions. We further assume that since 50 Ma, the crust and mantle have thickened homogeneously. Model B1 uses the "steady rise" elevation model to compute the thickness of the lithospheric mantle at 50 Ma. Incremental homogeneous thickening of the lithosphere since 50 Ma is assumed in order to match elevation in accordance with isostasy. Model B2 differs from B1 only in that the "rapid rise" elevation model is used instead of the "steady rise." A mantle lithosphere removal event by delamination thus corresponds to a jump from model B1 to A1, or B2 to A2.

[30] Finally we developed two more possible models, C1 and C2, using our shortening estimates at 21°S. We converted these shortening estimates into crustal thickening taking into account that the total crustal thickening includes the tectonic thickening due to the arc-normal shortening but also a minor component of arc-parallel tectonic shortening (10% of the arc-normal shortening [*Hindle et al.*, 2005, *Arriagada et al.*, 2008]) and magmatic thickening (up to 50% of the total tectonic thickening component in the arc-forearc region [*Haschke and Günther*, 2003]). Assuming that the crustal thickness was ~35 km at 50 Ma, it likely increased to ~60 km at present due to shortening (Figure 7b). This value is in good agreement with observations. In model C1 we assume that the 35-km thick crust was underlain by a ~30 km-thick lithospheric mantle at 50 Ma, and that thickening of the lithosphere was homogeneous since. Similarly, the initial value of the crustal thickness will affect the results. However, as mentioned above, only small variations of the crustal thickness are likely and these do not alter our results significantly.

[31] The resulting elevation calculated for model C1 via isostatic equilibrium gives ~500 m at 50 Ma and ~1000 m at 25 Ma. This estimate fits better the rapid rise elevation model but remains compatible with the lower end of the steady rise elevation model (Figure 7a). Elevation model C1 also gives a ~3000 m elevation at present-day, which is lower than the observed average ~3800 elevation for the internal plateau. In model C2, we assume that the crust was resting directly on the asthenosphere. The calculated elevations at 50 and 25 Ma are relatively high (~1000 and ~1500 m respectively), but agree well with the steady rise elevation model and remain compatible with predictions of the rapid rise model (Figure 7a). The model present-day elevation of ~3800 m fits well the observation for the internal plateau. As for the models derived directly from paleoelevation data, it is possible to construct a mixed scenario in which the mantle lithosphere is removed by delamination at some point in time as suggested by several studies

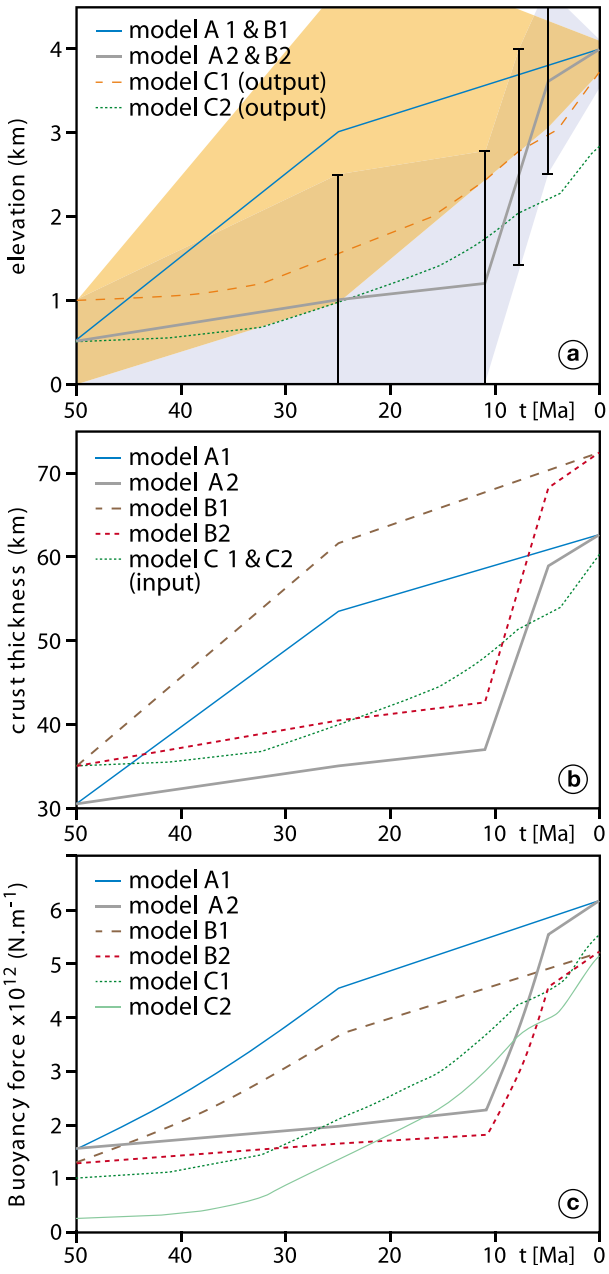

Figure 7. Possible scenarios for the evolution of elevation, crustal thickness and buoyancy force. (a) Paleoelevation evolution as summarized by *Barnes and Ehlers* [2009] showing the 'rapid rise' version (light gray shading) and the 'gradual rise' model (brown shading) in addition to two versions of paleoelevation reconstruction using the shortening record detailed in this study (see text for details). (b) Computed crustal thickness models based on the paleoelevation end-member models and shortening-based model. (c) Model results for buoyancy force evolution of crustal thickness models shown in Figure 7b. Assumptions and simplifications for each model are presented in Table 3.

[e.g., *Garzione et al.*, 2006, 2008; *Hoke and Garzione*, 2008]. Such an event would correspond to a subsequent jump from model C1 to C2.

[32] Integrating the difference in vertical traction between two lithospheric columns representing the central part of the orogen and the foreland, respectively, we compute the incremental increase of buoyancy force for each model. The shapes of the buoyancy force curves mimic the input parameters, either the elevation models or the crustal thickening model. All curves show an important increase of the buoyancy force from $<2 \times 10^{12}$ to $>5 \times 10^{12}$ N.m^{-1} (Figure 7c). Except for the rapid rise model (A2, B2) that shows a dramatic increase of buoyancy force between 10 and 6 Ma, all other models produce a rather gradual increase of force. The formation of the Subandean detachment with the observed increase of localization, acceleration of shortening, and increase of average fault slip rate occurring between 15 and 10 Ma hardly has a noticeable effect on plateau uplift from any of these models. The elevation curves derived from our shortening and thickening estimates show several points where plateau rise accelerates at ~32, ~14 Ma and 5 Ma. However, the curves are smooth and fit between the two end-member elevation models. Likewise there is no indication for a critical increase in buoyancy force at or before c. 15 Myr triggering localization toward the Subandean belt.

4.3. Constraining the Backarc Strength From Wedge Dynamics

[33] We indirectly constrain the strength evolution of the backarc wedge using observations that describe its first-order geometry. Critical taper mechanics [*Davis et al.*, 1983; *Dahlen et al.*, 1984; *Suppe*, 2007] provides an approach that allows estimating the strength of a basal detachment underlying the wedge and thereby controlling the crustal strength where the detachment penetrates most or all of the backarc crust. In the Central Andes, the Main Subandean Thrust (Figure 1) forms the basal detachment underlying the entire Subandean Thrust Belt at some 8–15 km depth. It extends westward over a distance of 250–300 km below the Eastern Cordillera where it is assumed to descend to >20 km depth toward the Moho [*Kley*, 1996; *Allmendinger and Zapata*, 2000]. *Allmendinger and Gubbels* [1996] first argued that formation of this detachment was instrumental in changing the deformation style at the Altiplano latitude (13–23°S) from pure shear to crustal-scale simple shear. Its development is possibly related to the presence of a thick pile of Lower Paleozoic shales

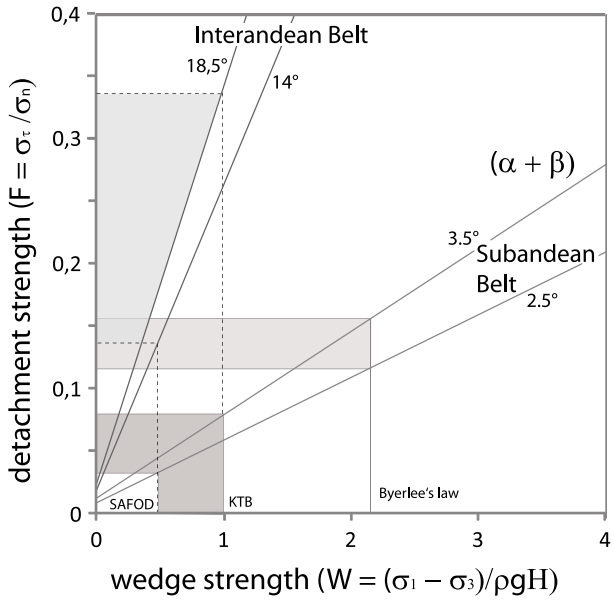

Figure 8. Estimated strength for detachment faults underlying the Subandean and Interandean belts. Calculation based on procedure from *Suppe* [2007] showing strength (effective basal friction, μ_b) for tapers between 18 and 22°S ($\alpha + \beta$ = 2.5 to 3.5°, and 18.5°), assuming hydrostatic conditions for the wedge. Wedge strength W shown for various values based on *Suppe* [2007] and references therein. Grey shaded areas provide range of strength values (F) resulting for Subandes and Interandes detachments using various values for the wedge strength.

[*Allmendinger and Gubbels*, 1996; *Kley*, 1996; *Oncken et al.*, 2006]. This is in contrast to the Puna latitude (23–28°S) where inversion structures and basement thrusting prevail [e.g., *Kley and Monaldi*, 2002].

[34] The Subandes exhibit a taper angle (surface slope and detachment dip ($\alpha + \beta$)) of 2.5–3° (Figure 1b) [*Allmendinger et al.*, 1997]. Using the small angle approximation, the normalized shear strength of the basal detachment may be estimated from [*Suppe*, 2007]:

$$\frac{\tau}{S_v} = \alpha\left(1 - \left(\frac{\rho_f}{\rho}\right)\right) + (\alpha + \beta)\frac{\sigma_1 - \sigma_3}{S_v}$$

where τ is shear strength of the detachment, S_v is vertical overburden stress, $\sigma_1 - \sigma_3$ is differential stress and ρ_f, ρ are fluid and rock densities, respectively. Assuming a depth of 10 km to the detachment below the Subandean (Figure 1b), hydrostatic pore pressure in the wedge and $\sigma_3 = Sv$, a wedge strength according to Byerlee's law (coefficient of friction: 0.85), for the small surface slope angles (0.5°–1°) in Northern Argentina and Southern Bolivia (18–22°S) we estimate an effective basal friction $\mu_b < 0.2$ (Figure 8). With even lower crustal strengths as found in deep continental drilling studies (KTB and SAFOD [see *Suppe*, 2007, and references therein]), we compute extremely weak effective basal detachment strengths of $\mu_b \approx 0.04$–0.07 (Figure 8). This value yields average shear stresses at the detachment level of 15–35 MPa providing an upper bound to the strength of the plateau-foreland transition for the present. Estimating the basal traction along the foreland detachment using the buoyancy forces yields average shear stresses of <25 MPa, which is in good agreement with our stress estimates using taper analysis.

[35] Wedge taper and strength prior to Subandean detachment formation – i.e., before the Middle to Late Miocene (see below) – are not constrained by direct observations. However, we note that the precursor décollement of the Subandes detachment, the Main Interandean detachment (Figure 1b), evolved around some 30 Ma and accumulated most deformation until some 10 Ma [*Ege et al.*, 2007]. Based on fission track data and an incremental restoration of the balanced section from *Kley* [1996], *Ege et al.* [2007] reconstruct the Interandean detachment geometry during the Miocene stage with a detachment dip (β) of around 12.5 to 17°. While surface slope (α) for this thrust system is not preserved we assume that the Miocene Interandean hanging wall slope was as or steeper than at present (i.e., 1–2°), since it now overlies the active and weak Subandes detachment. With these assumptions, we estimate a pre-Mid-Miocene effective coefficient of friction of $\mu_b \approx 0.15$–0.35 for the detachment level (Figure 8). Using the present-day detachment dip data for the Puna plateau latitude (13–17°) as determined by *Kley and Monaldi* [2002] from section balancing and the associated present surface slope (1.5–2°), we estimate that the current strength of the Puna flank is in the same range as the Mid-Miocene strength of the Altiplano flank (Figure 8). Hence, the strength of the plateau-foreland boundary has likely decreased substantially at the Altiplano latitude between Late Miocene and present. In contrast to strain localization and accelerated shortening observed at the Altiplano latitude, south of 23°S in the Puna region distributed basement thrusting prevails and shortening rates remained about constant until present.

5. Discussion

5.1. Strain Localization, Detachment Formation and Weakening

[36] The cumulative number of faults active during tectonic evolution of the Central Andes increased

monotonically. Fault numbers shows two distinct peaks between 30 and 25 Ma and at 15–10 Ma (Figure 5b). The first peak clearly correlates with a steep increase in deforming area in the plateau region (Figure 4b). It also correlates in time with a distinct increase in plate convergence rates between the Nazca plate and South America and with the onset of backarc magmatism. The first peak also correlates with the initiation of the first foreland-directed detachment, the Interandean thrust (see Figure 1b). The latter detachment became active around 30 Ma, as found from initiation of hangingwall cooling, kinematic analysis and section balancing [cf. *Kley*, 1996, *Müller et al.*, 2002, *Ege et al.*, 2007, *Barnes et al.*, 2008] and may reflect an early stage of foreland failure.

[37] Comparison of the second peak in fault activity with deforming area shows an inverse correlation marking the onset of localization at the plateau margin. This is also supported by the trend in average fault slip rate that started to increase during the same time interval. Employing sedimentological and thermochronological evidence, recent studies [e.g., *Barnes et al.*, 2008; *Uba et al.*, 2009] suggest that deformation in the hangingwall of the Subandes system started at some 15 Ma, extending earlier estimates of onset of deformation at around 10 Ma. Fault coalescence in the Subandean and the formation of a regionally coherent crustal detachment may therefore have set in and initiated localization at some 15–10 Ma. We also note that the reduction of number of active faults and the decrease of shortening rates within the plateau domain – during acceleration of shortening at the eastern flank – started at about 12 Ma lasting to around 7 Ma [*Elger et al.*, 2005]. During this time span fault slip rates accelerated from lower rates to slip rates one order of magnitude faster. Hence, we speculate that maturation of the Subandean detachment to form a throughgoing weak tabular fault zone of regional extent (13–23°S) took about 5–6 Myrs.

[38] Interestingly, plate convergence rates decreased concurrently from more than 12 cm/yr in the Middle Miocene [*Sdrolias and Müller*, 2006] to the present 6.6 cm/yr [*Angermann et al.*, 1999]. This suggests that increasing shortening rates of the upper plate are not linked to changes in plate convergence rates. From section balancing bulk horizontal strain in the upper crust of the Central Andes was 15–20% at about 10 Ma. To maintain strain compatibility, we expect a similar bulk strain down to lower crustal levels. This strain magnitude possibly defines a threshold for fault coalescence at depth and for formation of a throughgoing regional detachment. The formation of a coherent westward-dipping detachment that cuts through the entire upper and middle crust (Figure 1b) [see also *Allmendinger and Zapata*, 2000], alongside with deformation localization, is suggested to have been largely completed at about 7 Ma following its initiation at 15–10 Ma.

[39] We suggest that detachment formation is associated with a concurrent drop in backarc strength north of 23°S based on taper analysis of the Subandean belt. This decrease in backarc strength is accompanied by: a) increasing localization with eastward shift of deformation occurring in this time window, b) increasing average fault slip rates, as well as bulk shortening rates in spite of slowing plate convergence. We also note that stress orientation and present-day fault kinematics in the foreland east of the deformation front are decoupled from thrust fault kinematics in the overriding plate, also suggesting a weak detachment (e.g., Figure 2).

[40] It is interesting to note that plateau uplift and associated increase of buoyancy forces occurs in parallel with the decrease of taper angle and effective strength of the detachment. While the evolution of buoyancy forces shows no obvious relationship to weakening of the overriding plate and accelerated shortening, it may have played a role in shifting deformation and localization to the east as suggested by *Dalmayrac and Molnar* [1981]. However, note that the formation of the Interandean detachment at about 30 Myr occurred when plateau uplift had just started or elevation was still moderate. This clearly indicates that formation of a crustal-scale detachment is not related to buoyancy reaching a critical threshold value. Also, weakening, localization, and acceleration during the above period are obvious for the Altiplano latitudes only (north of 23°S), but not in the Puna region. Since the latter presumably exerts even higher buoyancy forces (Puna average elevation 4500 m versus 3800 m at the Altiplano latitude) the difference in Late Miocene to present evolution between both plateau domains is likely related to differences in geology and structural inventory of the Altiplano and Puna forelands, respectively.

[41] Finite shear strain of the Main Subandean detachment shear zone increases toward the Eastern Cordillera, where it is likely in excess of $\gamma > 50–100$ (estimated from balanced cross sections and assuming a maximum shear zone width of about 100 m). Studies of shear zone evolution in clay-rich and crystalline rocks deformed at very low up to amphibolite facies metamorphic conditions (i.e., brittle-ductile transition region) and experimental studies show that a

distinct foliation, significant grain size reduction and mineralogical changes commonly develop after average shear strains of <2–5 have accumulated [*Christiansen and Pollard*, 1997; *Fusseis et al.*, 2006; *Bos et al.*, 2000; *Rybacki et al.*, 2003; *Holyoke and Tullis*, 2006]. In these studies, fault fabrics forming in clay- or phyllosilicate-rich host rocks and gouges are found to significantly weaken faults resulting in lower friction, particularly in the presence of brine or water as a pore fluid [*Bos et al.*, 2000; *Collettini et al.*, 2009]. For the Subandean detachment, which formed in crystalline rocks at depth and Paleozoic shales in the brittle-ductile transition and brittle field, these findings from field and laboratory studies suggest that a mature fault fabric must have formed during the Late Miocene. For the significantly stronger detachment developing at the Puna latitude since some 5–6 Ma, largely within crystalline basement, similar shear strains were insufficient to weaken the fault system as for the Subandean detachment. Hence, we speculate that it requires shale-dominated host-rock lithologies to achieve the very low effective strength observed for the Subandean detachment system.

5.2. Alternative Weakening Mechanisms in the Andean Backarc?

[42] Several other mechanisms of weakening of the Andean arc/backarc system have been suggested in the past. *Isacks* [1988] [cf. also *Allmendinger et al.*, 1997] invoked thermal weakening from lithospheric thinning to have controlled backarc strength loss and initiation of deformation around 30–25 Ma (the so-called 'Andean crisis of *Sempéré et al.* [1990]). However, recent data show that deformation in the backarc area commenced during the Eocene, some 10–20 Myrs prior to the onset of magmatism [see *Oncken et al.*, 2006; *Barnes and Ehlers*, 2009, and references therein]. Moreover, patches of backarc magmatism show neither a spatial nor temporal correlation with domains of active deformation [*Trumbull et al.*, 2006], nor do variations in magmatic activity correlate with varying shortening rates [*Oncken et al.*, 2006]. Finally, the average fault slip rate trend (Figure 5c) remains stable during this entire period. Hence, our results at best support a weak influence of a thermal perturbation on the spatial distribution of deformation with, however, no effect on bulk shortening rate.

[43] Similar arguments pertain to the recent suggestion of massive backarc-wide delamination of mantle lithosphere supposedly having triggered rapid uplift of the Andean plateau surface and transfer of shortening from the plateau into the Subandean belt around 10–6.5 Myrs ago [e.g., *Garzione et al.*, 2006, 2008; *Hoke and Garzione*, 2008]. While this appears to be in agreement with the observation of very little mantle lithosphere material present underneath most of the Altiplano and the Puna [e.g., *Beck and Zandt*, 2002; *Schurr et al.*, 2006; *Tassara et al.*, 2006], it is at odds with the temporal evolution of shortening: The Subandes – and the acceleration to the modern shortening velocities – have started to form at c. 15 Ma, prior to the above suggested delamination and uplift event at 10–6.5 Ma. Moreover, the backarc magmatic activity as reconstructed and summarized by *Allmendinger et al.* [1997] and *Trumbull et al.* [2006] – presumably reflecting mantle lithosphere removal – reveals a protracted history of magmatism since 28 Ma with several peaks that show no temporal relation to the evolution of uplift and shortening. Finally, *Insel et al.* [2012] [see also *Ehlers and Poulsen*, 2009] have recalibrated the paleoaltimetric data, now including climate evolution, showing that Altiplano elevation has developed more gradually, akin to the shortening record reconstructed.

[44] Last, but not least, climate-driven erosional mass flux may have aided in focusing deformation on very few structures only in the Eastern Cordillera and Subandes. For the case of the southern Altiplano and its eastern flank, *Babeyko et al.* [2006] have shown numerically that the erosional flux here is well below the level where the above described effect may become relevant. For the northern Altiplano and its eastern flank, *Horton* [1999] interprets GPS data showing more distributed deformation as indicating erosional perturbation of critical wedge equilibrium. At the same time, we note that bulk shortening rates here are not significantly different from the more arid southern Altiplano. We therefore conclude that erosional weakening does not play a relevant role for the strength of the Andean lithosphere, but may influence the degree of localization of deformation in the hanging wall of the Subandes detachment [cf. also *Barnes et al.*, 2012].

[45] In summary, all of these alternative weakening mechanisms only take a secondary role and influence spatial distribution of deformation rather than temporal changes in strength. In fact, the overwhelming influence of upper plate weakening in the Andes by formation of a weak detachment system strongly corroborates the modeling-based parameter study by *Babeyko et al.* [2006] on the competition of various backarc weakening mechanisms.

5.3. Strain Localization Thresholds in Orogens And Rocks

[46] The evolving strain pattern in the Central Andes clearly shows that initially the area of active deformation increased relatively rapidly. However, deforming patches remained diffuse migrating in space and time prior to coalescence of a fault network involving <10 active shear zones starting not before the Late Miocene (Figure 5b). From the close correlation between the increase of actively deforming area and the growing active fault number (fault number active per time increment), we conclude that brittle faulting controls shortening at least in the upper crust across the entire Central Andes. Beyond a total horizontal strain of 20% the actively deforming area along the entire Altiplano decreased abruptly; progressive localization of shear strain into a small number of frontal thrusts started at about 15 Ma on the eastern flank. In contrast, across the Puna (23–27°S) the horizontal strain has only just attained approximately 20%. A laterally continuous basal detachment is still developing and we do not find a significant increase in average fault slip rate. These observations suggest that strain-related thresholds might exist on the scale of the continental lithosphere beyond which deformation modes change significantly.

[47] The recorded pattern of deformation is somewhat similar to what is observed in experimental studies of brittle rock fracture and friction. In some of these studies crack damage evolution is monitored using acoustic emissions (AE). These studies convincingly show that failure occurs after accumulation of spatially uncorrelated cracks distributed in the entire sample volume [e.g., *Lockner et al.*, 1991; *Stanchits et al.*, 2005]. Subsequently, failure is commonly initiated at a nucleation patch, which is likely affected by local heterogeneities of the material or an inhomogeneous stress field. Likewise, in high-strain torsion experiments performed at elevated temperatures and pressures, localization was mostly observed to occur in the presence of geometrical or material heterogeneities [e.g., *Rybacki et al.*, 2003].

[48] Plastic strain accumulated at brittle failure of rocks in tests at low temperatures and confining pressures is typically <3–5%. Instead, experiments performed in the semi-brittle and ductile regimes at elevated temperatures and pressures indicate that localization is often suppressed beyond strains in excess of 20% [e.g., *Evans et al.*, 1990; *Rybacki et al.*, 2003]. For deformation to remain localized in shear zones of finite width some form of slip weakening is commonly assumed. However, for semi-brittle and ductile deformation, only few laboratory and field studies exist that allow estimating quantitatively the amount of slip weakening induced during shear zone evolution [e.g., *Fusseis et al.*, 2006; *Pennacchioni and Mancktelow*, 2007; *Hansen et al.*, 2012]. Observational evidence highlights the role of a few key softening mechanisms such as grain size reduction, recrystallization, alignment of weak material components forming a pervasive fabric, reaction softening, shear zone coalescence and shear heating [e.g., *White et al.*, 1980; *Ben Zion and Sammis*, 2003; *Burlini and Bruhn*, 2006; *Handy et al.*, 2007; *Bürgmann and Dresen*, 2008; *Karato*, 2008]. Obviously, progressive strain localization on the scale of large shear zones or even a mountain belt is far more complex and precludes a simple transfer of experimental or small scale field observations [*Paterson*, 2001]. However, the above experimental data exhibit striking similarities in strain magnitude, geometric and kinematic patterns across a range of observational scales with the here presented Andean case (>8 orders of magnitude!) suggesting some form of scale invariance of tectonic strain accumulation.

[49] Finally, the change from low average fault slip rates to lithosphere-scale transient creep acceleration and weakening beyond c. 20% strain seems to stabilize in the Central Andes at higher slip rates since Pliocene times (Figure 5c). Our data show that localization and weakening are saturated at overall bulk strains of >30%. This value is surprisingly similar to numerical studies of fault networks involving slip weakening [*Spyropoulos et al.*, 2002]. Our analysis suggests that both, high constant shortening rates and stable degree of strain localization in the overriding plate are independent from plate convergence conditions. Instead, the recent stabilization at high rates is mainly governed by the reduced strength of the upper plate lithosphere and the evolution of a mature fault system.

6. Conclusions

[50] We find that Cenozoic strain accumulation in the Central Andes involved a complete cycle starting with spreading deformation across the entire overriding plate, which was followed after about 15 Ma by localization of deformation at the orogen scale. Interestingly, acceleration of shortening in the Andes correlated with waning plate convergence rates. The evolution of strain and strain rates is intimately tied to the growth and coalescence of fault networks leading ultimately to formation of crustal-scale detachment systems beyond a critical strain threshold of 15–20%. Moreover, geometric and geological analysis of the

detachment systems confining the Central Andes backarc suggests a substantial weakening of the eastern flank of the Andes. However, weakening only affected the Altiplano latitude of the Central Andes (13–22°S), but not the Puna latitude (22–28°S) where no significantly accelerated shortening and localization is observed. Weakening appears most closely associated to detachment formation in shale-dominated host-rock lithologies in the Subandean. Comparison of our observations with laboratory-based experimental analysis of rock deformation behavior in the brittle and the ductile fields exhibits some striking similarities: The evolution and characteristics of deformation and localization as well as the associated strain thresholds appear scale-invariant from the orogen to the laboratory specimen. We therefore note that the formation of the Central Andes is dominated by the strain accumulation history and the associated strength evolution of a rheologically layered lithosphere. Hence, the deformation record of an upper plate may serve as a suitable proxy to reconstruct its strength evolution. This implies that the deformation recorded in the upper plate may not allow constraining the external forcing mechanisms (i.e., variations in plate convergence, mantle-assisted processes, erosion, etc.) and how they may affect the evolution of a plate boundary system.

Acknowledgments

[51] A part of this study was developed during a stay of O.O. at CALTECH as a Moore fellow. A great number of people there and at GFZ have accompanied this study through discussion of our results. Last, but not least, J. Barnes and J. Loveless provided very detailed and thoughtful reviews that helped to clarify a number of issues and to significantly improve the readability of the manuscript. We thank all these colleagues for their collaboration and help.

References

Allmendinger, R. W., and T. Gubbels (1996), Pure and simple shear plateau uplift, Altiplano-Puna, Argentina and Bolivia, *Tectonophysics*, *259*(1–3), 1–13, doi:10.1016/0040-1951(96)00024-8.

Allmendinger, R. W., and T. R. Zapata (2000), The footwall ramp of the Subandean decollement, northernmost Argentina, from extended correlation of seismic reflection data, *Tectonophysics*, *321*(1), 37–55, doi:10.1016/S0040-1951(00)00077-9.

Allmendinger, R. W., T. E. Jordan, S. Mahlburg-Kay, and B. L. Isacks (1997), The evolution of the Altiplano-Puna Plateau of the Central Andes, *Annu. Rev. Earth Planet. Sci.*, *25*, 139–174, doi:10.1146/annurev.earth.25.1.139.

Allmendinger, R. W., R. Smalley Jr., M. Bevis, H. Caprio, and B. Brooks (2005), bending the Bolivian orocline in real time, *Geology*, *33*, 905–908, doi:10.1130/G21779.1.

Angermann, D., J. Klotz, and C. Reigber (1999), Space-geodetic estimation of the Nazca-South America Euler vector, *Earth Planet. Sci. Lett.*, *171*(3), 329–334.

Arriagada, C., P. Roperch, C. Mpodozis, and P. R. Cobbold (2008), Paleogene building of the Bolivian Orocline: Tectonic restoration of the central Andes in 2-D map view, *Tectonics*, *27*, TC6014, doi:10.1029/2008TC002269.

Babeyko, A. Y., S. V. Sobolev, T. Vietor, O. Oncken, and R. B. Trumbull (2006), Numerical study of the weakening processes in the Central Andean backarc, in *The Andes–Active Subduction Orogeny*, *Front. Earth Sci. Ser.*, vol. 1, edited by O. Oncken et al., pp. 495–512, Springer, Berlin.

Baby, P., G. Hérail, J. M. Lopez, J. Oller, J. Pareja, T. Sempéré, and D. Tufiño (1989), Structure de la Zone subandine de Bolivie: Influence de la géométrie des séries sédimentaires antéorogéniques sur la propagation de chevauchements, *C. R. Acad. Sci., Ser. II*, *309*, 1717–1722.

Baby, P., G. Hérail, R. Salinas, and T. Sempéré (1992), Geometry and kinematic evolution ofpassive roof duplexes deduced from cross section balancing: Example from the foreland thrust system of the southern Bolivian Subandean zone, *Tectonics*, *11*(3), 523–536, doi:10.1029/91TC03090.

Baby, P., B. Guillier, J. Oller, and G. Montemurro (1993), Modèle cinématique de la Zone subandine du coude de Santa Cruz (entre 16°S et 19°S, Bolivie) déduit de la construction de cartes equilibrées, *C. R. Acad. Sci., Ser. II*, *317*, 1477–1483.

Baby, P., P. Rochat, G. Mascle, and G. Hérail (1997), Neogene shortening contribution to crustal thickening in the back arc of the Central Andes, *Geology*, *25*(10), 883–886, doi:10.1130/0091-7613(1997)025<0883:NSCTCT>2.3.CO;2.

Barnes, J. B., and T. A. Ehlers (2009), End member models for Andean Plateau uplift, *Earth Sci. Rev.*, *97*(1–4), 105–132, doi:10.1016/j.earscirev.2009.08.003.

Barnes, J. B., T. A. Ehlers, N. McQuarrie, P. B. O'Sullivan, and J. D. Pelletier (2006), Eocene to recent variations in erosion across the central Andean fold-thrust belt, northern Bolivia: Implications for plateau evolution, *Earth Planet. Sci. Lett.*, *248*(1–2), 118–133.

Barnes, J. B., T. A. Ehlers, N. McQuarrie, P. B. O'Sullivan, and S. Tawackoli (2008), Thermochronometer record of central Andean plateau growth, Bolivia (19.5°S), *Tectonics*, *27*, TC3003, doi:10.1029/2007TC002174.

Barnes, J. B., T. A. Ehlers, N. Insel, N. McQuarrie, and C. J. Poulsen (2012), Linking orography, climate, and exhumation across the central Andes, *Geology*, *40*(12), 1135–1138, doi:10.1130/G33229.1.

Beck, S. L., and G. Zandt (2002), The nature of orogenic crust in the central Andes, *J. Geophys. Res.*, *107*(B10), 2230, doi:10.1029/2000JB000124.

Ben-Zion, Y., and C. G. Sammis (2003), Characterization of fault zones, *Pure Appl. Geophys.*, *160*(3–4), 677–715, doi:10.1007/PL00012554.

Bevis, M., E. Kendrick, R. Smalley, B. Brooks, R. Allmendinger, and B. Isacks (2001), On the strength of interplate coupling and the rate of back arc convergence in the central Andes: An analysis of the interseismic velocity field, *Geochem. Geophys. Geosyst.*, *2*(11), 1067, doi:10.1029/2001GC000198.

Bos, B., C. J. Peach, and C. J. Spiers (2000), Frictional-viscous flow of simulated fault gouge caused by the combined effects of phyllosilicates and pressure solution, *Tectonophysics*, *327*(3–4), 173–194, doi:10.1016/S0040-1951(00)00168-2.

Boutelier, D., and O. Oncken (2010), Role of the plate margin curvature in the plateau build-up: Consequences for the Central Andes, *J. Geophys. Res.*, *115*, B04402, doi:10.1029/2009JB006296.

Brooks, B. A., M. Bevis, R. Smalley, E. Kendrick, R. Manceda, E. Lauria, R. Maturana, and M. Araujo (2003), Crustal motion in the Southern Andes (26°–36°S): Do the Andes behave like a microplate?, *Geochem. Geophys. Geosyst.*, *4*(10), 1085, doi:10.1029/2003GC000505.

Brooks, B. A., et al. (2011), Orogenic-wedge deformation and potential for great earthquakes in the central Andean backarc, *Nat. Geosci.*, *4*, 380–383, doi:10.1038/ngeo1143.

Bürgmann, R., and G. Dresen (2008), Rheology of the lower crust and upper mantle: Evidence from rock mechanics, geodesy, and field observations, *Annu. Rev. Earth Planet. Sci.*, *36*, 531–567, doi:10.1146/annurev.earth.36.031207.124326.

Burlini, L., and D. Bruhn (2006), High-strain zones; Laboratory perspectives on strain softening during ductile deformation, *Geol. Soc. Spec. Publ.*, *245*, 1–24.

Capitanio, F. A., C. Faccenna, S. Zlotnik, and D. R. Stegman (2011), Subduction dynamics and the origin of Andean Orogeny and the Bolivian Orocline, *Nature*, *480*(7375), 83–86, doi:10.1038/nature10596.

Carrapa, B., D. Adelmann, G. E. Hilley, E. Mortimer, E. R. Sobel, and M. R. Strecker (2005), Oligocene range uplift and development of plateau morphology in the southern Central Andes, *Tectonics*, *24*, TC4011, doi:10.1029/2004TC001762.

Carrapa, B., J. D. Trimble, and D. F. Stockli (2011), Patterns and timing of exhumation and deformation in the Eastern Cordillera of NW Argentina revealed by (U-Th)/He thermochronology, *Tectonics*, *30*, TC3003, doi:10.1029/2010TC002707.

Charrier, R., A. N. Chavez, S. Elgueta, G. Herail, J. J. Flynn, D. A. Croft, A. R. Wyss, R. Riquelme, and M. Garcia (2005), Rapid tectonic and paleogeographic evolution associated with the development of the Chucal anticline and the Chucal-Lauca Basin in the Altiplano of Arica, northern Chile, *J. South Am. Earth Sci.*, *19*, 35–54, doi:10.1016/j.jsames.2004.06.008.

Chase, C. G., A. J. Sussman, and D. D. Coblentz (2009), Curved Andes; Geoid, forebulge, and flexure, *Lithosphere*, *1*(6), 358–363, doi:10.1130/L67.1.

Christiansen, P. P., and D. D. Pollard (1997), Nucleation growth and structural development of mylonitic shear zones in granitic rock, *J. Struct. Geol.*, *19*(9), 1159–1172, doi:10.1016/S0191-8141(97)00025-4.

Cladouhos, T. T., R. W. Allmendinger, B. Coira, and E. Farrar (1994), Late Cenozoic deformation in the central Andes: Fault kinematics from the northern Puna, northwestern Argentina and southwestern Bolivia, *J. South Am. Earth Sci.*, *7*(2), 209–228, doi:10.1016/0895-9811(94)90008-6.

Collettini, C., A. Niemeijer, C. Viti, and C. Marone (2009), Fault zone fabric and fault weakness, *Nature*, *462*(7275), 907–910, doi:10.1038/nature08585.

Coutand, I., A. Chauvin, P. R. Cobbold, P. Gautier, and P. Roperch (1999), Vertical axis rotations across the Puna plateau (northwestern Argentina) from paleomagnetic analysis of Cretaceous and Cenozoic rocks, *J. Geophys. Res.*, *104*(B10), 22,965–22,984, doi:10.1029/1999JB900148.

Coutand, I., P. R. Cobbold, M. de Urreiztieta, P. Gautier, A. Chauvin, D. Gapais, E. A. Rossello, and O. López-Gamundí (2001), Style and history of Andean deformation, Puna plateau, northwestern Argentina, *Tectonics*, *20*(2), 210–234, doi:10.1029/2000TC900031.

Cowie, P. A., J. R. Underhill, M. D. Behn, J. Lin, and C. E. Gill (2005), Spatio-temporal evolution of strain accumulation derived from multi-scale observations of Late Jurassic rifting in the northern North Sea: A critical test of models for lithospheric extension, *Earth Planet. Sci. Lett.*, *234*(3–4), 401–419.

Cristallini, E., A. H. Cominguez, and V. A. Ramos (1997), Deep structure of the Metan-Guachipas region; Tectonic inversion in northwestern Argentina, *J. South Am. Earth Sci.*, *10*(5–6), 403–421, doi:10.1016/S0895-9811(97)00026-6.

Dahlen, F. A., J. Suppe, and D. Davis (1984), Mechanics of fold-and-thrust belts and accretionary wedges: Cohesive Coulomb Theory, *J. Geophys. Res.*, *89*(B12), 10,087–10,101, doi:10.1029/JB089iB12p10087.

Dalmayrac, B., and P. Molnar (1981), Parallel thrust and normal faulting in Peru and constraints on the state of stress, *Earth Planet. Sci. Lett.*, *55*(3), 473–481, doi:10.1016/0012-821X(81)90174-6.

Davis, D., J. Suppe, and F. A. Dahlen (1983), Mechanics of fold-and-thrust belts and accretionary wedges, *J. Geophys. Res.*, *88*(B2), 1153–1172, doi:10.1029/JB088iB02p01153.

DeMets, C., R. G. Gordon, D. F. Argus, and S. Stein (1990), Current plate motions, *Geophys. J. Int.*, *101*(2), 425–478, doi:10.1111/j.1365-246X.1990.tb06579.x.

Devlin, S., B. L. Isacks, M. E. Pritchard, W. D. Barnhart, and R. B. Lohman (2012), Depths and focal mechanisms of crustal earthquakes in the central Andes determined from teleseismic waveform analysis and InSAR, *Tectonics*, *31*, TC2002, doi:10.1029/2011TC002914.

Drury, M. R., and J. L. Urai (1990), Deformation-related recrystallization processes, *Tectonophysics*, *172*(3–4), 235–253, doi:10.1016/0040-1951(90)90033-5.

Dunn, J. F., K. G. Hartshorn, and P. W. Hartshorn (1995), Structural styles and hydrocarbon potential of the Subandean thrust belt of southern Bolivia, in *Petroleum Basins of South America*, edited by A. J. Tankard, R. S. Soruco, and H. J. Welsink, *AAPG Mem.*, *62*, 523–543.

Ege, H., E. R. Sobel, E. Scheuber, and V. Jacobshagen (2007), Exhumation history of the southern Altiplano plateau (southern Bolivia) constrained by apatite fission-track thermochronology, *Tectonics*, *26*, TC1004, doi:10.1029/2005TC001869.

Ehlers, T. A., and C. J. Poulsen (2009), Influence of Andean uplift on climate and paleoaltimetry estimates, *Earth Planet. Sci. Lett.*, *281*(3–4), 238–248.

Elger, K., O. Oncken, and J. Glodny (2005), Plateau-style accumulation of deformation–the Southern Altiplano, *Tectonics*, *24*, TC4020, doi:10.1029/2004TC001675.

Engdahl, E. R., R. van der Hilst, and R. Buland (1998), Global teleseismic earthquake relocation with improved travel times and procedures for depth determination, *Bull. Seismol. Soc. Am.*, *88*, 722–743.

Evans, B., J. T. Fredrich, and T. F. Wong (1990), The brittle-ductile transition in rocks: Recent experimental and theoretical progress, in *The Brittle-Ductile Transition in Rocks*, *Geophys. Monogr. Ser.*, vol. 56, edited by A. G. Duba et al., pp. 1–20, AGU, Washington, D. C., doi:10.1029/GM056p0001.

Froidevaux, C., and B. L. Isacks (1984), The mechanical state of the lithosphere in the Altiplano-Puna segment of the Andes, *Earth Planet. Sci. Lett.*, *71*(2), 305–314, doi:10.1016/0012-821X(84)90095-5.

Fusseis, F., M. R. Handy, and C. Schrank (2006), Networking of shear zones at the brittle-to-viscous transition (Cap de Creus, NE Spain), *J. Struct. Geol.*, *28*(7), 1228–1243, doi:10.1016/j.jsg.2006.03.022.

García, M., G. Hérail, R. Charrier, G. Mascle, M. Fornani, and C. P. de Arce (2002), Oligocene-Neogene tectonic evolution of the Altiplano of Northern Chile (18–19°S), paper presented at Fifth International Symposium on Andean Geodynamics, Univ. Paul Sabatier, Toulouse, France.

Garzione, C. N., P. Molnar, J. C. Libarkin, and B. J. MacFadden (2006), Rapid late Miocene rise of the Bolivian Altiplano: Evidence for removal of mantle lithosphere, *Earth Planet. Sci. Lett.*, *241*, 543–556, doi:10.1016/j.epsl.2005.11.026.

Garzione, C. N., G. D. Hoke, J. C. Libarkin, S. Withers, B. MacFadden, J. Eiler, P. Ghosh, and A. Mulch (2008), Rise of the Andes, *Science*, *320*(5881), 1304–1307, doi:10.1126/science.1148615.

Gerbi, C., N. Culshaw, and J. Marsh (2010), Magnitude of weakening during crustal-scale shear zone development, *J. Struct. Geol.*, *32*(1), 107–117, doi:10.1016/j.jsg.2009.10.002.

Ghosh, P., C. N. Garzione, and J. M. Eiler (2006), Rapid uplift of the Altiplano revealed through ^{13}C-^{18}O bonds in paleosol carbonates, *Science*, *311*(5760), 511–515, doi:10.1126/science.1119365.

Gregory-Wodzicki, K. M. (2000), Uplift history of the Central and Northern Andes: A review, *Geol. Soc. Am. Bull.*, *112*(7), 1091–1105, doi:10.1130/0016-7606(2000)112<1091:UHOTCA>2.0.CO;2.

Grier, M. E., J. A. Salfity, and R. W. Allmendinger (1991), Andean reactivation of the Cretaceous Salta rift, northwestern Argentina, *J. South Am. Earth Sci.*, *4*(4), 351–372, doi:10.1016/0895-9811(91)90007-8.

Handy, M. R., G. Hirth, and R. Bürgmann (2007), Continental fault structure and rheology from the frictional-to-viscous transition downward, in *Tectonic Faults–Agents of Change on a Dynamic Earth*, edited by M. R. Handy et al., pp. 139–182, MIT Press, Cambridge, Mass.

Hansen, L. N., M. E. Zimmerman, A. M. Dillman, and D. L. Kohlstedt (2012), Strain localization in olivine aggregates at high temperature: A laboratory comparison of constant-strain-rate and constant-stress boundary conditions, *Earth Planet. Sci. Lett.*, *333–334*, 134–145, doi:10.1016/j.epsl.2012.04.016.

Haschke, M., and A. Günther (2003), Balancing crustal thickening in arcs by tectonic vs. magmatic means, *Geology*, *31*(11), 933–936, doi:10.1130/G19945.1.

Heidbach, O., M. Tingay, A. Barth, J. Reinecker, D. Kurfess, and B. Müller (2010), Global crustal astress pattern based on the World Stress Map database release 2008, *Tectonophysics*, *482*, 3–15, doi:10.1016/j.tecto.2009.07.023.

Hérail, G., P. Baby, M. López, J. Oller, O. López, R. Salinas, T. Sempéré, G. Beccar, and H. Toledo (1990), Structure and kinematic evolution of Subandean thrust system, Bolivia, paper presented at First International Symposium on Andean Geodynamics, Univ. Joseph Fourier, Grenoble, France.

Hérail, G., J. Oller, P. Baby, M. Bonhomme, and P. Soler (1996), Strike-slip faulting, thrusting and related basins in the Cenozoic evolution of the southern branch of the Bolivian Orocline, *Tectonophysics*, *259*(1–3), 201–212.

Hindle, D., J. Kley, O. Oncken, and S. V. Sobolev (2005), Crustal flux and crustal balance from shortening in the Central Andes, *Earth Planet. Sci. Lett.*, *230*, 113–124, doi:10.1016/j.epsl.2004.11.004.

Hobbs, B. E., H. B. Muhlhaus, and A. Ord (1990), Instability, softening and localization of deformation, in *Deformation Mechanisms, Rheology and Tectonics*, edited by R. Knipe and E. H. Rutter, *Geol. Soc. Spec. Publ.*, *54*, 143–165.

Hoke, G. D., and C. N. Garzione (2008), Paleosurfaces, paleoelevation, and the mechanisms for the late Miocene topographic development of the Altiplano plateau, *Earth Planet. Sci. Lett.*, *271*(1–4), 192–201.

Holyoke, C. W., III, and J. Tullis (2006), Formation and maintenance of shear zones, *Geology*, *34*(2), 105–108, doi:10.1130/G22116.1.

Horton, B. K. (1999), Erosional control on the geometry and kinematics of thrust belt development in the Central Andes, *Tectonics*, *18*(6), 1292–1304, doi:10.1029/1999TC900051.

Husson, L., and Y. Ricard (2004), Stress balance above subduction; Application to the Andes, *Earth Planet. Sci. Lett.*, *222*(3–4), 1037–1050.

Iaffaldano, G., and H. P. Bunge (2008), Strong plate coupling along the Nazca-South America convergent margin, *Geology*, *36*(6), 443–446, doi:10.1130/G24489A.1.

Insel, N., C. J. Poulsen, T. A. Ehlers, and C. Sturm (2012), Response of meteoric delta O-18 to surface uplift - Implications for Cenozoic Andean Plateau growth, *Earth Planet. Sci. Lett.*, *317-318*, 262–272, doi:10.1016/j.epsl.2011.11.039.

Isacks, B. L. (1988), Uplift of the Central Andean Plateau and bending of the Bolivian Orocline, *J. Geophys. Res.*, *93*(B4), 3211–3231, doi:10.1029/JB093iB04p03211.

Jordan, T. E., P. L. Nester, N. Blanco, G. D. Hoke, F. Davila, and A. J. Tomlinson (2010), Uplift of the Altiplano-Puna plateau: A view from the west, *Tectonics*, *29*, TC5007, doi:10.1029/2010TC002661.

Karato, S. (2008), *Deformation of Earth Materials; An Introduction to the Rheology of Solid Earth*, 463 pp., Cambridge Univ. Press, Cambridge, U. K., doi:10.1017/CBO9780511804892.

Kendrick, E., M. Bevis, R. Smalley Jr., and B. Brooks (2001), An integrated crustal velocityfield for the central Andes, *Geochem. Geophys. Geosyst.*, *2*(11), 1066, doi:10.1029/2001GC000191.

Kley, J. (1996), Transition from basement-involved to thin-skinned thrusting in the CordilleraOriental of southern Bolivia, *Tectonics*, *15*(4), 763–775, doi:10.1029/95TC03868.

Kley, J., and C. R. Monaldi (1998), Tectonic shortening and crustal thickness in the Central Andes: How good is the correlation?, *Geology*, *26*(8), 723–726, doi:10.1130/0091-7613(1998)026<0723:TSACTI>2.3.CO;2.

Kley, J., and C. R. Monaldi (2002), Tectonic inversion in the Santa Barbara System of the central Andean foreland thrust belt, north-western Argentina, *Tectonics*, *21*(6), 1061, doi:10.1029/2002TC902003.

Klotz, J., A. Abolghasem, G. Khazaradze, B. Heinze, T. Vietor, R. Hackney, K. Bataille, R. Maturana, J. Viramonte, and R. Perdomo (2006), Long-term signals in the present day deformation field of the Central and Southern Andes and constraints on the viscosity of the earth's upper mantle, in *The Andes–Active Subduction Orogeny*, *Front. Earth Sci. Ser.*, vol. 1, edited by O. Oncken et al., pp. 65–90, Springer, Berlin.

Lamb, S. (2000), Active deformation in the Bolivian Andes, South America, *J. Geophys. Res.*, *105*(B11), 25,627–25,653, doi:10.1029/2000JB900187.

Lamb, S. (2006), Shear stresses on megathrusts: Implications for mountain building behind subduction zones, *J. Geophys. Res.*, *111*, B07401, doi:10.1029/2005JB003916.

Lamb, S., and L. Hoke (1997), Origin of the high plateau in the Central Andes, Bolivia, South America, *Tectonics*, *16*(4), 623–649.

Lockner, D. A., J. D. Byerlee, V. Kuksenko, A. Ponomarev, and A. Sidorin (1991), Quasi-static fault growth and shear fracture energy in granite, *Nature*, *350*(6313), 39–42, doi:10.1038/350039a0.

Lyakhovsky, V., Y. Ben-Zion, and A. Agnon (2001), Earthquake cycle, fault zones, and seismicity patterns in a rheologically layered lithosphere, *J. Geophys. Res.*, *106*(B3), 4103–4120, doi:10.1029/2000JB900218.

Marrett, R. A., R. W. Allmendinger, R. N. Alonso, and R. E. Drake (1994), Late Cenozoic tectonic evolution of the Puna Plateau and adjacent foreland, north-western Argentine Andes, *J. South Am. Earth Sci.*, *7*(2), 179–207, doi:10.1016/0895-9811(94)90007-8.

McLeod, A. E., N. H. Dawers, and J. R. Underhill (2000), The propagation and linkage of normal faults: Insights from the Strathspey-Brent-Statfjord fault array, northern North Sea, *Basin Res.*, *12*(3–4), 263–284, doi:10.1046/j.1365-2117.2000.00124.x.

McQuarrie, N., and P. DeCelles (2001), Geometry and structural evolution of the Central Andean backthrust belt, Bolivia, *Tectonics*, *20*(5), 669–692, doi:10.1029/2000TC001232.

McQuarrie, N., J. B. Barnes, and T. A. Ehlers (2008), Geometric, kinematic, and erosional history of the central Andean Plateau, Bolivia (15–17°S), *Tectonics*, *27*, TC3007, doi:10.1029/2006TC002054.

Meade, B. J., and C. P. Conrad (2008), Andean growth and the deceleration of South American subduction: Time evolution of a coupled orogen-subduction system, *Earth Planet. Sci. Lett.*, *275*(1–2), 93–101.

Mercier, J. L., M. Sébrier, A. Lavenu, J. Cabrera, O. Bellier, J. F. Dumont, and J. Machare (1992), Changes in the tectonic regime above a subduction zone of Andean type: The Andes of Peru and Bolivia during the Pliocene-Pleistocene, *J. Geophys. Res.*, *97*(B8), 11,945–11,982, doi:10.1029/90JB02473.

Molnar, P., and H. Lyon-Caen (1988), Some simple physical aspects of the support, structure, and evolution of mountain belts, *Spec. Pap. Geol. Soc. Am.*, *218*, 179–207.

Müller, J. P., J. Kley, and V. Jacobshagen (2002), Structure and Cenozoic kinematics of the Eastern Cordillera, southern Bolivia (21°S), *Tectonics*, *21*(5), 1037, doi:10.1029/2001TC001340.

Muñoz, N., and R. Charrier (1996), Uplift of the western border of the Altiplano on a westvergentthrust system, northern Chile, *J. South Am. Earth Sci.*, *9*(3–4), 171–181, doi:10.1016/0895-9811(96)00004-1.

Oncken, O., D. Hindle, J. Kley, K. Elger, P. Victor, and K. Schemmann (2006), Deformation of the Andean upper plate system–Facts, fiction, and constraints for modellers, in *The Andes–Active Subduction Orogeny*, *Front. Earth Sci. Ser.*, vol. 1, edited by O. Oncken et al., pp. 3–28, Springer, Berlin.

Paterson, M. S. (1978), *Experimental Rock Deformation; The Brittle Field*, 254 pp., Springer, Berlin.

Paterson, M. S. (2001), Relating experimental and geological rheology, *Int. J. Earth Sci.*, *90*(1), 157–167, doi:10.1007/s005310000158.

Pennacchioni, G., and N. S. Mancktelow (2007), Nucleation and initial growth of a shear zone network within compositionally and structurally heterogeneous granitoids under amphibolite facies condition, *J. Struct. Geol.*, *29*(11), 1757–1780, doi:10.1016/j.jsg.2007.06.002.

Rodriguez, W. G., P. Baby, and J. Ballard (2001), Structure and palaeogeographic control of the Peruvian Subandean zone, *C. R. Acad. Sci., Ser. IIa*, *333*, 741–748.

Roeder, D., and R. L. Chamberlain (1995), Structural geology of sub-Andean fold and thrust belt in Northwestern Bolivia, in *Petroleum Basins of South America*, edited by A. J. Tankard, R. S. Suárez, and H. J. Welsink, *AAPG Mem.*, *62*, 459–479.

Rousse, S., S. Gilder, M. Fornari, and T. Sempéré (2005), Insight into the Neogene tectonic history of the northern Bolivian Orocline from new paleomagnetic and geochronologic data, *Tectonics*, *24*, TC6007, doi:10.1029/2004TC001760.

Ruiz, G. M. H., V. Carlotto, P. V. van Heinigen, and P. A. M. Andriessen (2009), Steady-state exhumation pattern in the Central Andes; SE Peru, *Geol. Soc. Spec. Publ.*, *324*, 307–316, doi:10.1144/SP324.20.

Rybacki, E., M. S. Paterson, R. Wirth, and G. Dresen (2003), Rheology of calcite-quartz aggregates deformed to large strain in torsion, *J. Geophys. Res.*, *108*(B2), 2089, doi:10.1029/2002JB001833.

Scheuber, E., and K. J. Reutter (1992), Magmatic arc tectonics in the Central Andes between 21 and 25°S, *Tectonophysics*, *205*, 127–140, doi:10.1016/0040-1951(92)90422-3.

Schildgen, T. F., K. V. Hodges, K. X. Whipple, M. S. Pringle, M. van Soest, and K. Cornell (2009), Late Cenozoic structural and tectonic development of the western margin of the central Andean Plateau in southwest Peru, *Tectonics*, *28*, TC4007, doi:10.1029/2008TC002403.

Scholz, C. H. (2002), *The Mechanics of Earthquakes and Faulting*, 2nd ed., 471 pp., Cambridge Univ. Press, Cambridge, U. K., doi:10.1017/CBO9780511818516.

Schurr, B., A. Rietbrock, G. Asch, R. Kind, and O. Oncken (2006), Evidence for lithospheric detachment in the central Andes from local earthquake tomography, *Tectonophysics*, *415*(1–4), 203–223, doi:10.1016/j.tecto.2005.12.007.

Sdrolias, M., and R. D. Müller (2006), Controls on back-arc basin formation, *Geochem. Geophys. Geosyst.*, *7*, Q04016, doi:10.1029/2005GC001090.

Sempéré, T., G. Hérail, J. Oller, and M. G. Bonhomme (1990), Late Oligocene Early Miocene major tectonic crisis and related basins in Bolivia, *Geology*, *18*(10), 946–949, doi:10.1130/0091-7613(1990)018<0946:LOEMMT>2.3.CO;2.

Sheffels, B. M. (1990), Lower bound on the amount of crustal shortening in the central Bolivian Andes, *Geology*, *18*, 812–815, doi:10.1130/0091-7613(1990)018<0812:LBOTAO>2.3.CO;2.

Sobolev, S. V., and A. Y. Babeyko (2005), What drives orogeny in the Andes?, *Geology*, *33*(8), 617–620, doi:10.1130/G21557.1.

Spyropoulos, C., C. H. Scholz, and B. E. Shaw (2002), Transition regimes for growing crack populations, *Phys. Rev.*, *65*, 056105, doi:10.1103/PhysRevE.65.056105.

Stanchits, S., S. Vinciguerra, and G. Dresen (2005), Ultrasonic velocities, acoustic emission characteristics and crack damage of basalt and granite, *Pure Appl. Geophys.*, *163*(5–6), 974–993.

Suppe, J. (2007), Absolute fault and crustal strength from wedge tapers, *Geology*, *35*(12), 1127–1130, doi:10.1130/G24053A.1.

Tassara, A., H. J. Götze, S. Schmidt, and R. Hackney (2006), Three-dimensional density model of the Nazca plate and Andean continental margin, *J. Geophys. Res.*, *111*, B09404, doi:10.1029/2005JB003976.

Trumbull, R. B., U. Riller, O. Oncken, E. Scheuber, K. Munier, and F. Hongn (2006), The time-space distribution of Cenozoic volcanism in the South-Central Andes: A new data compilation and some tectonic implications, in *The Andes–Active Subduction Orogeny*, *Front. Earth Sci. Ser.*, vol. 1, edited by O. Oncken et al., pp. 29–44, Springer, Berlin.

Uba, C. E., J. Kley, M. R. Strecker, and A. K. Schmitt (2009), Unsteady evolution of the Bolivian Subandean thrust belt: The role of enhanced erosion and clastic wedge progradation, *Earth Planet. Sci. Lett.*, *281*(3–4), 134–146.

Vauchez, A., A. Tommasi, and D. Mainprice (2012), Faults (shear zones) in the Earth's mantle, *Tectonophysics*, *558–559*, 1–27, doi:10.1016/j.tecto.2012.06.006.

Victor, P., O. Oncken, and J. Glodny (2004), Uplift of the western Altiplano Plateau: Evidence from the Precordillera between 20°S and 21°S; northern Chile, *Tectonics*, *23*, TC4004, doi:10.1029/2003TC001519.

Vietor, T., and H. P. Echtler (2006), Episodic Neogene southward growth of the Andean subduction orogen between 30°S and 40°S; plate motions, mantle flow, climate, and upper-plate structure, in *The Andes–Active Subduction Orogeny*, *Front. Earth Sci. Ser.*, vol. 1, edited by O. Oncken et al., pp. 375–400, Springer, Berlin.

Vissers, R. L. M., M. R. Drury, E. H. Hoogerduijn Strating, C. J. Spiers, and D. van der Wal (1995), Mantle shear zones and their effect on lithosphere strength during continental breakup, *Tectonophysics*, *249*(3–4), 155–171, doi:10.1016/0040-1951(95)00033-J.

White, S. H., S. E. Burrows, J. Carreras, N. D. Shaw, and F. J. Humphreys (1980), On mylonites in ductile shear zones, *J. Struct. Geol.*, *2*(1-2), 175–187, doi:10.1016/0191-8141(80)90048-6.

Yuan, X., et al. (2000), Subduction and collision processes in the Central Andes constrained by converted seismic phases, *Nature*, *408*, 958–961, doi:10.1038/35050073.